Resonant Multiphoton Fragmentation Spectrum of Niobium Dimer Cation

ARTICLE *in* THE JOURNAL OF PHYSICAL CHEMISTRY A · MARCH 2009

Impact Factor: 2.69 · DOI: 10.1021/jp809089y · Source: PubMed

2 AUTHORS, INCLUDING:

Metin Aydin
Ondokuz Mayıs Üniversitesi
32 PUBLICATIONS **171** CITATIONS

Article

Resonant Multiphoton Fragmentation Spectrum of Niobium Dimer Cation

M. Aydin, and John R. Lombardi

J. Phys. Chem. A, **2009**, 113 (12), 2809-2820• DOI: 10.1021/jp809089y • Publication Date (Web): 19 February 2009

Resonant Multiphoton Fragmentation Spectrum of Niobium Dimer Cation

M. Aydin*,† and John R. Lombardi‡

Department of Chemistry, Faculty of Art and Sciences, Ondokuz Mayıs University, 55139 Samsun, Turkey, and Department of Chemistry and Center for Analysis of Structures and Interfaces (CASI), The City College of New York (CCNY), New York, New York 10031

Received: October 14, 2008; Revised Manuscript Received: January 12, 2009

Resonant multiphoton fragmentation spectra of niobium dimer cation (Nb_2^+) have been obtained by utilizing laser vaporization of a Nb metal target. Ions are mass-selected with a time-of-flight mass spectrometer followed by a mass gate and then fragmented with a pulsed dye laser, and the resulting fragment ions are detected with a second time-of-flight reflectron mass spectrometer and multichannel plate. Photon resonances are detected by monitoring ion current as a function of fragmentation laser wavelength. A rich but complex spectrum of the cation is obtained. The bands display a characteristic multiplet structure that may be interpreted as due to transitions from the ground state $X^4\Sigma^-_{\Omega g}$ to several excited states, $(B/D)^4\Pi_{\Omega u}$ and $^4\Sigma^-_{\Omega u}$. The ground state $X^4\Sigma^-_{\pm 1/2g}$ is derived from the electron configuration $\pi_u{}^4 1\sigma_g{}^2 2\sigma_g{}^1 \delta_g{}^2$. The two spin−orbit components are split by 145 cm^{-1} due to a strong second-order isoconfigurational spin−orbit interaction with the low-lying $^2\Sigma^+_{\pm 1/2g}$ state. The vibrational frequencies of the ground sate and the excited-state of Nb_2^+ are identified as well as molecular spin−orbit constants (A_{SO}) in the excited state. The electronic structure of niobium dimer cation was investigated using density functional theory. For the electronic ground state, the predicted spectroscopic properties were in good agreement with experiment. Calculations on excited states reveal congested manifolds of quartet and doublet electronic states in the range 0−30 000 cm^{-1}, reflecting the multitude of possible electronic promotions among the 4d- and 5s-based molecular orbitals. Comparisons are drawn between Nb_2^+ and the prevalent isoelectronic molecules $V_2^+/NbV^+/Nb_2/V_2/NbV_2$.

I. Introduction

The ionic and neutral transition metal clusters have received special interest since the advent of techniques such as laser vaporization of a solid target, supersonic cooling, mass-selected resonant two-photon ionization, laser-induced fluorescence, and collision-induced dissociation.[1−27] The transition metal clusters are an area of active research because of their potential applications in homogeneous and heterogeneous catalysis, nanoparticals, etc. It is important to understand how the metal−metal bonding properties, the catalytic selectivity, stability, and mechanism change as a function of cluster size. However, even in the diatomic transition metal clusters, there are some major difficulties associated with their investigation. For instance, the electronic structures and bonding energies of the diatomic molecules remain a challenge for both experimentalists and theoreticians. The difficulty in the characterization of their spectroscopic properties originates from their partially occupied d-orbitals that produce many low-lying electronic states and cause large electron correlation as well as a strong first- and second-order spin−orbit coupling effects.

We focus here on analyzing the one-color multiphoton fragmentation spectrum for Nb_2^+ produced through laser vaporization. With accessible particle counting techniques, it is possible to detect cluster ions with near-unit efficiency, and as a consequence, absorption spectra of a mass-selected cluster ion can be readily obtained using high peak intensity probe lasers. Both one and multiphoton absorption spectra and the dissociation energy limit can be studied with high sensitivity.[2c,19,24,25] For a multiphoton process, a molecule with energy in excess of its lowest dissociation threshold can dissociate given enough time, assuming that there exist no barriers in excess of the threshold. The probability or normalized intensity of fragment cluster ions is not only inversely proportional to the number of photons absorbed by the parent ion (Nb_2^+) but also the bound−bound transition resonant enhancement of the multiphoton fragmentation of the parent ion maximum at the absorption of the first photon in the multiphoton fragmentation spectrum. Therefore, the possible dipole-allowed electronic transitions of the parent ion can be obtained from a sharp rise of features in the spectral background of the fragmented niobium ion (Nb^+) when the multiphoton fragmentation is monitored as a function of probe photon energy. The order of the resonance multiphoton process for the Nb_2^+ cation have been determined to be three-photon processes in the 16 000−18 500 cm^{-1} region by the fluence dependence study in our pervious work,[25] a collision-induced dissociation (CID) experiment,[23] and density functional calculations (DFT) at the BLYP/Lanl2dz level.[25,26]

In 1985, the first experimental observation of the multiphoton fragmentation spectroscopy of Nb_2^+, in the 17 850−18 200 cm^{-1} region, had been reported by Smalley et al.[27] In this region, their spectra exhibit many features similar to ours, except for a mismatch of 100 cm^{-1} in wavelength, and some peaks observed in their spectrum are very weak or disappear in ours. A recalibration of our laser using a mercury lamp and a Spex 'Doublemate' monochromator showed our laser to be off by only 0.15 nm or about 5 cm^{-1}; therefore, the possibility exists that their laser may have been blue-shifted

* To whom correspondence should be addressed. E-mail: aydn123@netscape.net.
† Ondokuz Mayıs University.
‡ The City College of New York.

10.1021/jp809089y CCC: $40.75
Published on Web 02/19/2009

as much as 100 cm^{-1}. In 1994, an ESR study on Nb_2^+ in argon matrices by Weltner et al.[28] suggested that the ground-state of Nb_2^+ was $^2\Sigma_g^+$, arising from the electronic configuration $1\pi_u^4 1\sigma_g^2 2\sigma_g^1 \delta_g^2$. However, all theoretical calculations such as the density functional theory (DFT), [25,26,29] complete active space self-consistent field (CASSCF),[30] complete active space self-consistent field calculations followed by multi-reference configuration interaction (CASSCF/MRCI), and a more recent spin−orbit configuration interaction (SOCI) calculations using the intermediate neglect of differential overlap method for optical spectroscopy (INDO/S)[31] predicted $^4\Sigma_g^-$ as a ground-state of Nb_2^+, arising from the same electronic configuration $1\pi_u^4 1\sigma_g^2 2\sigma_g^1 \delta_g^2$, consistent with Hund's rule.

To the best of our knowledge, no experimental value for the second-order spin−orbit splitting (Δ) has been reported, except for a few theoretical calculations. The first reported Δ value for Nb_2^+ calculated by Simard et al.[29] is 142 cm^{-1}, which is in good agreement with the calculations at the different levels of the DFT (109, 119, and 166 cm^{-1}) by Aydin et al.[26] and 145 cm^{-1} from INDO/S-SOCI calculations by O'Brien.[31] However, Balasubramanian and Zhu have performed the FOCI at the CASSCF/MRCI level and they found 18 low-lying electronic states below 16 900 cm^{-1}. Their calculations predicted that $^2\Sigma_{\bar{\Omega}g}^-$ lies about 5000 cm^{-1} above the ground state, but no $^2\Sigma_{\bar{\Omega}g}^+$ state is found within 16 900 cm^{-1} of the ground state. However, the $X^4\Sigma_{\bar{\Omega}g}$ [$...\delta_g^+(\alpha)\delta_g^-(\alpha)2\sigma_g(\alpha)$] and $^2\Sigma_{\bar{\Omega}g}$ [$...\delta_g^+(\alpha)\delta_g^-(\alpha)2\sigma_g(\beta)$] electronic states of Nb_2^+ arise as a consequence of the coupling of the $2\sigma_g(\alpha)$ and $2\sigma_g(\beta)$ electrons to the $\delta_g^+(\alpha)\delta_g^-(\alpha)(X^3\Sigma_{\bar{\Omega}g}^-)$ open-shell configuration of the Nb_2, respectively. The $^2\Sigma_{\bar{\Omega}g}^+$ [$...\delta_g^+(\alpha)\delta_g^-(\beta)2\sigma_g(\alpha)$] symmetry results from the coupling of the $2\sigma_g(\alpha)$ to the $\delta_g^+(\alpha)\delta_g^-(\beta)(^1\Sigma_{\bar{\Omega}g}^+)$ open-shell configurations of the Nb_2. Since the measured distance between the $^1\Sigma_{0g}^+$ and $X^3\Sigma_{0g}^-$ states of Nb_2 by Simard et al.[10] (from the rotationally well-resolved R2PI spectra of Nb_2) is about 2000 cm^{-1}, we expect that the $^2\Sigma_{\bar{\Omega}g}^+$ [$...\delta_g^+(\alpha)\delta_g^-\beta)(^1\Sigma_{0g}^+)\otimes 2\sigma_g(\alpha)$] low-lying state of Nb_2^+ should not be too far from its ground state, $X^4\Sigma_{\bar{\Omega}g}^-$ [$...\delta_g^+(\alpha)\delta_g^-(\alpha)(^3\Sigma_{0g}^-)\otimes 2\sigma_g(\alpha)$].

The course of our experiment determines the second-order splitting in the ground-state and first-order splitting in the excited states of the Nb_2^+ in addition to other spectroscopic constants.

II. Calculations on Niobium Dimer Cation

A. Ground Sate. A review by Lombardi and Davis[24] has already summarized experimentally determined force constants (k), internuclear distances (R), and their corresponding ground-state symmetries from first-row through third-row transition metals. In the literature, there are also many theoretical works carried out on the ground- and excited-state properties of homonuclear and heteronuclear neutral and ionic dimer molecules of the transition metal at different level of the theories. Even though the theoretical calculations do not precisely predict the bonding energies and vibrational frequencies or force constants of the transition metal dimer molecules, they may provide useful information about the electronic configuration and ground and excited-state symmetries of the transition metals in order to explain most of the experimental results. The error in the predicted vibrational frequencies in the ground-state of the dimer molecules are expected to be less than about 15%. In some cases, based on the theory used, it may be more or less than this error range. Since the predicted force constants or vibrational frequencies for transition metals show similar trends along a series of transition metal dimer molecules, such as along a group or a period/row in the periodic table, it can be corrected using a scaling factor by fitting to their corresponding experimental values as used in organic compounds. One of the aims of the present work, using DFT methods at same level of theory, BLYP/LanL2DZ level, for the neutral and ionic dimer molecules all considered here is to predict their force constants and obtain theoretical evidence as to whether the theoretical results indicate an analogous trend with regard to the corresponding experimental values. For a few dimer molecules, such as Mn_2, Zn_2, and Cd_2, the BLYP/LanL2DZ predicted internuclear distances that are far from the experimental values. In order to improve the results, we tried a different type of basis set than LanL2DZ. The CEP-121G basis function produced consistent results for these dimers. Second, we are concerned here with how their ground-state symmetries and the force constants (k) as well as their equilibrium internuclear distances (R) at their ground states change when these molecules are ionized.

Due to availability of the ground-state properties of the neutral dimer molecules, in order to test the reliability of the methods, first we calculated the force constants, ground-state electronic configuration or symmetries, and internuclear distances for the neutral transition dimer molecules at their ground states from first row through third row. Then, we used the same method to calculate those parameters for their corresponding ionic species in their ground states. As shown in Table 1, the calculated force constants and internuclear distances are well-correlated with their corresponding experimental values. Their predicted ground-state symmetries also are consistent with their experimentally and theoretically well-known ground-state symmetries, except Ni_2. The calculation predicted the ground state of the Ni_2 to be $^3\Delta_g$, arising from the $\pi_g^4\delta_u^3\sigma_u^1$. However, there is a low-lying state $^3\Sigma_g(\delta_u^4\pi_g^2\sigma_u^2)$, which lies just 55 cm^{-1} above the $^3\Delta_g$ state. If the second-order spin−orbit splitting between the $^3\Sigma_g^-$−$^1\Sigma_g^+$ states is larger than first order spin−orbit splitting in the $^3\Delta_g$ state, then the $^3\Sigma_g(\delta_u^4\pi_g^2\sigma_u^2)$ may be expected to be the ground-state of the Ni_2.

Fitting the experimental force constants vs corresponding calculated ones, we obtained the following fitting equations: k(exp./first row) = 0.715k(calc/first row), with error = 2.9% and R = 0.987; k(exp./second row) = 0.886k(calc/second row), with error = 8.8% and R = 0.97; k(exp./third row) = 0.908k(calc/third row), with error = 4.5% and R = 0.97. The calculations overestimated the force constant of the Cr_2, even though the predicted internuclear distance is consistent with its experimental value. When we attempted to calculate the singlet ground state [$^1\Sigma_g^+$ ($...2\sigma_g^2\delta_g^4$)] potential energy curve to a Morse potential energy curve, we were unsuccessful. However, as mentioned in ref 24, due to a substantial distortion of the potential function, its actual potential energy curve shape is a shelf-like potential instead of a Morse potential. On the other hand, the ground-state may not consist of a single electronic configuration, $...2\sigma_g^2\delta_g^4$, and there might be a significant isoconfigurational interaction contribution to the ground state. Therefore, in order to obtain the best fitting, we ignored Cr_2 in the first row in addition to Tc_2 in the second row. The fitting of the experimental internuclear distances to corresponding calculated ones gives the following equations: R(exp./first row) = 0.989R(calc/first row), with error = 0.6%; R(exp./second row) = 0.986k(calc/second row), with error = 1.2%. For third row transition metal dimer molecules, we do not have enough experimental data on the internuclear distance to compare with the calculated ones. Their predicted ground-state term symbols and R and k values are in agreement with the experimental finding, as seen in Table 1.

TABLE 1: Calculated Ground-State Neutral and Ionic Transition-Metal Dimer Molecules from First Row to Third Row, Term Symbol,[b] Internuclear Distances (Å), Vibrational Frequencies (cm^{-1}), and Force Constants (mdyn/Å)[a,c]

		Sc_2			Ti_2			V_2			Cr_2			Mn_2	
sym	$^4\Delta_g$	$^5\Sigma_u$	$^2\Sigma_g$	$^4\Delta_u$	$^3\Delta_g$	4	$^4\Sigma_g$	$^3\Sigma_g$	$^4\Sigma_u$	$^2\Sigma_g$	$^1\Sigma_g$	$^2\Sigma_u$	2	1	2
R	2.751	2.651	2.251	2.227	1.951	1.977	1.750	1.791	1.804	1.629	1.652	1.667	2.368	2.960	2.694
ω	241	241	305	340	462	428	710	642	607	772	749	711	213	83	129
k	0.769	0.767	1.233	1.629	3.020	2.582	7.566	6.187	5.530	9.128	8.590	7.734	0.734	0.112	0.268
exp.[a]		$^5\Sigma_u$			$^3\Delta_g$		$^4\Sigma_g$	$3\Sigma_g$			$^1\Sigma_g$			$^1\Sigma_g$	
R_{exp}					1.942			1.77			1.679			3.4	
k_{exp}		0.76			2.35			4.33			3.54			0.09	
		Y_2			Zr_2			Nb_2			Mo_2			Tc_2	
sym	$^4\Sigma_g$	$^5\Sigma_u$	$^2\Pi_u$	$^2\Sigma_g$	$^3\Delta_g$	$^2\Delta_g$	$^4\Sigma_g$	$^3\Sigma_g$	$^4\Sigma_u$	$^4\Sigma_g$	$^1\Sigma_g$	$^2\Sigma_u$	$^4\Sigma_g$	$^1\Gamma_g/^1\Sigma_g$	$^2\Sigma_u$
R	2.874	2.960	2.805	2.377	2.336	2.304	2.121	2.157	2.184	1.994	2.006	2.023	2.041	2.030	2.052
ω	200	180	194	259	311	360	436	444	416	500	524	500	453	486	417
k	1.048	0.847	0.982	1.781	2.568	3.433	5.202	5.402	4.733	7.223	7.934	7.208	6.033	6.982	6.278
exp.	$^4\Sigma_g$	$^5\Sigma_u$			$^3\Delta_g$			$^3\Sigma_g$			$^1\Sigma_g$			–	
R_{exp}					2.24			2.078			1.929				
k_{exp}		0.89			2.51			4.84			6.33			4.37	
		La_2			Hf_2			Ta_2			W_2			Re_2	
sym	$^4\Sigma_g$	$^1\Sigma_g$	$^2\Sigma_g$	$^2\Sigma_g$	$^3\Sigma_u$	$^2\Sigma_g$	$^2\Delta_g$	$^5\Sigma_u$	$^4\Sigma_u$	$^4\Delta_u$	$^1\Sigma_g$	$^2\Sigma_u$	$^4\Delta_g$	$^3\Delta_g$	$^4\Sigma_u$
R	3.255	2.962	2.922	2.380	2.438	2.505	2.220	2.289	2.220	2.175	2.065	2.092	2.125	2.086	2.119
ω	138	147	182	244	223	200	326	272	302	345	387	365	361	372	350
k	0.780	0.881	1.350	3.147	2.6397	2.120	5.673	3.941	4.868	6.458	8.129	7.201	7.159	7.606	6.750
exp.		–			–			–			$\{^1\Sigma_g\}$			$^3\Delta_g$	
R_{exp}															
		Fe_2			Co_2			Ni_2			Cu_2			Zn_2	
k_{exp}		2.28			1.63			4.80			6.14			6.26	
sym	$^6\Delta_u$	$^7\Delta_u$	$^6\Delta_g$	6	5	4	4	$^3\Delta_g{}^3\Sigma_g$	2	2	$^1\Sigma_g$	$^2\Sigma_u$	$^2\Sigma_u$	$^1\Sigma_g$	$^2\Sigma_u$
R	2.135	2.043	2.087	2.115	2.145	2.186	2.251	2.146	2.206	2.387	2.247	2.364	2.611	3.442	6.437
ω	351	398	362	345	340	296	292	315	279	205	264	199	148	27	16
k	2.029	2.617	2.164	2.062	2.007	1.518	1.453	1.699	1.333	0.778	1.289	0.735	0.414	0.014	0.005
exp.		$\{^7\Delta_u\}$			$\{^5\Delta_u\}$			0_g			$^1\Sigma_g$			$^1\Sigma_g$	
R_{exp}		2.02						2.154			2.22			4.19	
k_{exp}		1.48			1.53			1.16			1.33			0.01	
		Ru_2			Rh_2			Pd_2			Ag_2			Cd_2	
sym	$^6\Sigma_u$	$^7\Delta_u$	$^6\Sigma_g/^6\Gamma_g$	$^6\Delta_g$	$^5\Sigma_u$	6	$^2\Sigma_u$	$^3\Sigma_u$	$^2\Sigma_u$	$^2\Sigma_g$	$^1\Sigma_g$	$^2\Sigma_u$	$^2\Sigma_u$	$^1\Sigma_g$	$^2\Sigma_g$
R	2.378	2.309	2.310	2.333	2.348	2.326	2.677	2.539	2.496	2.794	2.616	2.779	2.979	4.010	5.770
ω	266	315	300	278	273	278	150	198	203	126	174	126	99	18	11
k	2.128	2.980	2.702	2.348	2.259	2.347	0.701	1.223	1.285	0.503	0.967	0.503	0.332	0.011	0.004
exp.		$\{^7\Delta_u\}$			$\{^5\Delta_{u,g}\}$			$\{^3\Sigma_u\}$			$^1\Sigma_g$			$^1\Sigma_g$	
R_{exp}											2.53			4.07	
k_{exp}		3.59			2.44			1.38			1.18			0.02	
		Os_2			Ir_2			Pt_2			Au_2			Hg_2	
sym	$^4\Sigma_u$	$^5\Pi_u$	$^2\Delta_u$	$^2\Sigma_u$	3	$^4\Delta_u$	$^4\Pi_u$	$^3\Sigma_g$	$^4\Sigma_g$	$^2\Sigma_g$	$^1\Sigma_g$	$^2\Sigma_u$	$^2\Sigma_u$	$^1\Sigma_g$	$^2\Pi_u$
R	2.134	2.186	2.169	2.186	2.285	2.314	2.485	2.400	2.476	2.701	2.588	2.756	3.262	4.193	3.703
ω	349	322	330	315	268	253	192	220	187	131	156	109	55	13	25
k	6.803	5.802	6.076	5.657	4.088	3.629	2.122	2.771	2.004	1.003	1.420	0.686	0.180	0.009	0.037
exp.		–			–			0_g			$^1\Sigma_g$			$^1\Sigma_g$	
R_{exp}								2.33			2.47			3.69	
k_{exp}		6.26			4.44			2.84			2.12			0.02	

[a] The experimental values are taken from ref 24, except for V_{2+} and Y_{2+} are respectively taken from references 34 and 7. [b] The symmetry for a few ionic and neutral species were not determined due to their partially occupied d-orbitals; thus, only spin multiplicities ($2S + 1$) are given in the sym row. [c] The columns under each molecule indicate cation, neutral, and anion, respectively.

As a result, the calculation indicated that DFT theory at BLYP/LanL2DZ level predicts the force constants and internuclear distances in an acceptable error range for each row transition metal series. On the other hand, they are well-correlated with their corresponding experimental values,[24] DFT calculations at different level of theory,[16] and the results of the universal three-parameter potential energy function calculations,[15] but they are superior to the results of the previous DFT calculations, at PW86/DZVP-LDA and PW86/DZVP-GGA levels, by Calaminici et al.[14]

The calculated force constants for each of the cationic and anionic transition metals showed an analogous trend when compared with their corresponding neutral ones. A plot was made of the logarithmic values of these calculated force constants vs their corresponding interatomic distances (R) according to Pauling's rule.[32] The R dependence of the logarithmic values of these calculated force constants, $\ln(k)$, provided similar linear equations for each set of data as given below. For the first row: $\ln(k$; exp./neutral$) = 5.36 - 2.35R$ (Å); $\ln(k$; calc/neutral$) = 5.77 - 2.36R$ (Å); $\ln(k$; calc/cation)

TABLE 2: Calculated Singlet and Triplet Electronic Energy Levels of Nb_2 at TD-BLYP/LanL2DZ Level

sym	transition	configuration[a]	R_e (Å)	ω_e (cm^{-1})	T_e (cm^{-1})
$X^3\Sigma_g^-$		$(\pi_u)^4(1\sigma_g2\sigma_g)^4(\delta_g)^2$	2.157	444	0
$^1\Gamma_g$		$(\pi_u)^4(1\sigma_g2\sigma_g)^4(\delta_g)^2$	2.170	440	560
$^1\Sigma_g^+$		$(\pi_u)^4(1\sigma_g2\sigma_g)^4(\delta_g)^2$	2.165	446	2 400
$^1\Delta_g(1)$	$\sigma_g\rightarrow\delta_g$	$(\pi_u)^4(1\sigma_g2\sigma_g)^3(\delta_g)^3$	2.065	445	5 690
$^3\Delta_g(1)$	$\sigma_g\rightarrow\delta_g$	$(\pi_u)^4(1\sigma_g2\sigma_g)^3(\delta_g)^3$	2.192	450	6 500
$^3\Gamma_u$	$\delta_g\rightarrow\delta_u$	$(\pi_u)^4(1\sigma_g)^2(2\sigma_g)^1(\delta_g)^1(\delta_u*)^1$	2.262	380	7 700
$^3\Delta_g(2)$	$\sigma_g\rightarrow\sigma_u$	$(\pi_u)^4(1\sigma_g2\sigma_g)^3(\delta_g)^3$	2.172	590	8 500
$^3\Phi_u(1)$	$\pi_u\rightarrow\delta_g$	$(\pi_u)^3(1\sigma_g2\sigma_g)^4(\delta_g)^3$	2.225	390	8 800
$^3\Delta_u(1)$	$\delta_g\rightarrow\delta_u$	$(\pi_u)^4(1\sigma_g2\sigma_g)^4(\delta_g)^1(\sigma_u*)^1$	2.245	410	9 800
$^3\Sigma_u(1)$	$\sigma_g\rightarrow\sigma_u$	$(\pi_u)^4(1\sigma_g2\sigma_g)^3(\delta_g)^2(\sigma_u*)^1$	2.150	390	10 650
$^3\Sigma_u^+(2)$	$\delta_g\rightarrow\delta_u$	$(\pi_u)^4(1\sigma_g2\sigma_g)^4(\delta_g)^1(\delta_u*)^1$	2.290	340	10 900
$^3\Sigma_u(3)$	$\sigma_g\rightarrow\sigma_u$	$(\pi_u)^4(1\sigma_g2\sigma_g)^3(\delta_g)^2(\sigma_u*)^1$	2.255	460	11 350
$^3\Pi_u(1)$	$\pi_u\rightarrow\delta_g$	$(\pi_u)^3(1\sigma_g2\sigma_g)^4(\delta_g)^3$	2.218	400	11 500
$^1\Delta_u(1)$	$\delta_g\rightarrow\delta_u$	$(\pi_u)^4(1\sigma_g2\sigma_g)^4(\delta_g)^1(\delta_u*)^1$	2.235	426	12 300
$^1\Delta_g(1)$	$\sigma_g\rightarrow\delta_g$	$(\pi_u)^4(1\sigma_g2\sigma_g)^3(\delta_g)^3$	2.186	474	12 500
$^3\Delta_u(2)$	$\sigma_g\rightarrow\delta_u$	$(\pi_u)^4(1\sigma_g2\sigma_g)^3(\delta_g)^2(\sigma_u*)^1$	2.221	330	12 300
$^1\Pi_u(1)$	$\pi_u\rightarrow\delta_g$	$(\pi_u)^3(1\sigma_g2\sigma_g)^4(\delta_g)^3$	2.225	388	13 700
$^3\Pi_g(1)$	$\pi_u\rightarrow\sigma_u$	$(\pi_u)^3(1\sigma_g2\sigma_g)^4(\delta_g)^2(\sigma_u*)^1$	2.325	350	14 250
$^3\Sigma_u(4)$	$\sigma_g\rightarrow\sigma_u$	$(\pi_u)^4(1\sigma_g2\sigma_g)^3(\delta_g)^2(\sigma_u*)^1$	2.230	350	14 250
$^1\Gamma_u$	$\delta_g\rightarrow\delta_u$	$(\pi_u)^4(1\sigma_g2\sigma_g)^4(\delta_g)^1(\delta_u*)^1$	2.245	425	14 400
$^3\Phi_g(1)$	$\pi_u\rightarrow\delta_u$	$(\pi_u)^3(1\sigma_g2\sigma_g)^4(\delta_g)^2(\delta_u*)^1$	2.328	330	14 700
$^3\Sigma_u(5)$	$\sigma_g\rightarrow\sigma_u$	$(\pi_u)^4(1\sigma_g2\sigma_g)^3(\delta_g)^2(\sigma_u*)^1$	2.245	450	15 300

* Each excited-state results from more than one electronic isoconfigurational interaction, but only the dominant part of the isoelectronic configuration is provided here.

$= 6.40 - 2.67R$ (Å); $\ln(k;$ calc/anion$) = 7.74 - 3.37R$ (Å). For the second row: $\ln(k;$ exp./neutral$) = 7.06 - 2.70R$ (Å); $\ln(k;$ calc/neutral$) = 8.41 - 3.12R$ (Å); $\ln(k;$ calc/cation$) = 7.67 - 2.90R$ (Å); $\ln(k;$ calc/anion$) = 8.11 - 3.06R$ (Å). For the third row: $\ln(k;$ exp./neutral$) = 9.81 - 3.71R$ (Å); $\ln(k;$ calc/neutral$) = 8.60 - 3.13R$ (Å); $\ln(k;$ calc/cation$) = 7.49 - 2.64R$ (Å); $\ln(k;$ calc/anion$) = 8.58 - 3.13R$ (Å). In the present work, we mainly focused on Nb_2^+ and briefly summarize calculated results of the ground-state properties of the neutral and ionic homomolecules. Comprehensive calculated results on the ground-state spectroscopic properties of these species, including their heteromolecules, are in preparation and will be published elsewhere.

The ground-state symmetry of Nb_2^+ is predicted to be $X^4\Sigma_g^-$ symmetry, resulting from the $...1\pi_u^4 1\sigma_g^2 2\sigma_g^1 1\delta_g^2$ open-shell electronic configuration. The predicted ground-state vibrational frequency (ω_e) and interatomic distance (R_e) are respectively 436 cm^{-1} and 2.120 Å, in agreement with our previous calculations at different levels of the DFT theory[26] and with the calculations at the FOCI level.[30]

B. Calculated Electronic Energy Levels of Nb_2^+. Calculations for excited-state configurations were performed by using time-dependent density functional theory (TD-DFT) at the TD-BLYP/Lanl2DZ level of the theory for at least 15 values of the interatomic distance ranging between 1.95 and 2.35 Å. Additional calculations were performed to predict T_e and R_e values by separately optimizing every electronic state considered. Then, in order to estimate ω_e for each electronic state, the SCF-corrected TD-BLYP transition energies were fitted to the experimentally known dissociation energy of the Nb_2^+ by using a potential energy function that is given by[33]

$$D(X) = D_e[(1 - e^{-\beta X})^2 + c\beta^3X^3(1 + b\beta X)e^{-\beta X}]$$

where $X = R - R_e$, $\beta = 1.2177 \times 10^7\omega_e(\mu/D_e)^{1/2}$, the values of ω_e and $D_e(=D_e(Nb_2^+,X^4\Sigma_g^-) - T_e)$ are in cm^{-1} units, and μ is the reduced mass in amu. The b and c parameters were taken as variable at each fitting procedure, but their exact definitions can be found in ref 33. It should be noticed that the TD-DFT technique only allows configurational interactions resulting from one-electron excitations for each desired excited state, not (the configurational interactions result from) double or higher electron excitations. Nevertheless, for transition metals, in some cases, especially over about 2 eV, double or higher electronic excitation may play an important role for certain electronic states. In such cases, we used the transition state optimization (opt-TS) technique for desired electronic configurations, $^4\Pi$ ($\pi_u^2 1\sigma_g^2 2\sigma_g^2 \delta_g^3$) and $^4\Pi$ ($\pi_u^2 1\sigma_g^2 2\sigma_g^2 \delta_g^3$) transition states, for at least twenty values of the interatomic distance ranging between 1.95 and 2.35 Å. The opt-TS method requests optimization to a desired transition state rather than a local minimum and does not include configurational interactions (CI). Therefore, the calculated values may be expected to be somewhat higher than a calculated value from a method considering CI such as the MRCI technique. Furthermore, the doublet-electronic configurations of Nb_2^+ produce many low-lying electronic states, but two low-lying sates can be derived from the electronic configuration $...\pi_u^4 1\sigma_g^2 2\sigma_g^1(\alpha)\delta_g^2(\alpha\beta)$ with $^2\Gamma_g$ and $^2\Sigma_g^+$ symmetry. A single set of spectroscopic properties is computed for these two states, which are indistinguishable. In order to distinguish these two states, we again used opt-TS techniques to determine which of them correspond to the $^2\Gamma_g$ or $^2\Sigma_g^+$ symmetry by replacing the occupied $\delta_g^1(\beta)$ orbital with the unoccupied $\delta_g*(\beta)$ orbital for 20 values of the interatomic distance ranging between 1.95 and 2.4 Å.

In order to test the reliability of the calculations, at first, we calculated electronic energy levels of the triplet and singlet energy levels of the Nb_2. The calculated dipole-allowed electronic transitions of Nb_2 are consistent with its rotationally resolved spectrum and previous DFT calculations by Simard et al.[10,29] and the FOCI calculations by Balasubramanian and Zhu,[30] as seen in Table 2 and Figure 1. Balasubramanian and Zhu[30] also calculated 18 low-lying states below 16 900 cm^{-1} for Nb_2^+ at the FOCI level, as mentioned earlier. Their calculation showed that there are four $X^4\Sigma_g^- \rightarrow {}^4\Pi_u$ dipole-allowed electronic transitions, but only two of the four $^4\Pi_u$ transitions lie in our observed

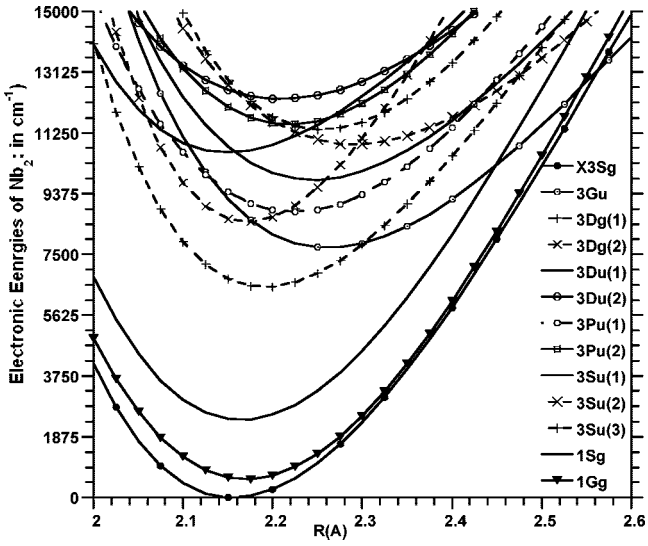

Figure 1. The calculated triplet- and singlet-energy levels of the Nb_2 at BLYP/LanL2DZ level of the DFT.

spectral region of Nb_2^+, henceforth termed as $A^4\Pi_u$ (ca., T_e = 16 328 cm^{-1}) and $B^4\Pi_u$ (ca., T_e = 16 882 cm^{-1}) states. Their major valence electronic configurations are respectively $1\sigma_g^1\pi_u^3 2\sigma_g^1\delta_g^4$ (21.7%) + $1\sigma_g^2\pi_u^3 2\sigma_g^1\delta_g^3$ (32.2%) and $1\sigma_g^1\pi_u^3 2\sigma_g^1\delta_g^4$ (31.0%) + $1\sigma_g^2\pi_u^3 2\sigma_g^1\delta_g^3$ (26.4%).[30]

The TD-DFT calculations predicted many low-lying transitions for the quartet and doublet states of the Nb_2^+. In Tables 2 and 3 we provided the calculated excited states of the neutral and ionic niobium dimer molecules, respectively. We would like to point out that each excited state given in Tables 2 and 3 results from more than one electronic isoconfigurational interaction, but only the dominant part of the isoelectronic configuration is provided for each excited-state symmety in the tables. For instance, the $^4\Pi_u(1)$ excited state (at 7862 cm^{-1}) is the result of the single excitations from the ground state ($\pi_u^4 1\sigma_g^2 2\sigma_g^1\delta_g^2$) to the $\pi_u^3 1\sigma_g^2 2\sigma_g^2\delta_g^2$ (dominant) + $\pi_u^3 1\sigma_g^2 2\sigma_g^1\delta_g^3$ (minor) electronic states and the transition to the $\pi_u^3 1\sigma_g^2 2\sigma_g^2\delta_g^2$ (minor) + $\pi_u^3 1\sigma_g^2 2\sigma_g^1\delta_g^3$ (dominant) for the $^4\Pi_u(2)$ excited-state at 12 920 cm^{-1}. As seen in Table 3 and Figure 2, the TD-DFT calculations produced two $X^4\Sigma_g^- \rightarrow {}^4\Pi_u$ dipole-allowed electronic transitions, 7863 and 12 920 cm^{-1}, as a result of the $\pi_u \rightarrow 2\sigma_g/\delta_g$ transitions and two others around 30 000 cm^{-1} that are due to $2\sigma_g/\delta_g \rightarrow \pi_u^*$ transitions. The calculations also predicted three strong $X^4\Sigma_g^- \rightarrow {}^4\Sigma_u^-$ transitions at 16 000/17 900/17 990 cm^{-1} in the observed multiphoton fragmentation spectral region of Nb_2^+. No $X^4\Sigma_g^- \rightarrow {}^4\Pi_u$ transition was predicted in the range 16 000−18 500 cm^{-1}. In this case, we used the opt-TS technique to the investigate existence of any $^4\Pi_u$state in the regions of 16 000−19 000 cm^{-1}. Even though the TS method does not take account of configuration interaction (CI), the calculation produced four $X^4\Sigma_g^- \rightarrow {}^4\Pi_u$ transitions when higher excitations are involved in calculations such as $^4\Pi_u(3)$ $[(\pi_u)^3(1\sigma_g 2\sigma_g)^4(\delta_u)^2]$ with T_e = 21 270 cm^{-1}, $^4\Pi_u(4)$ $[(\pi_u)^3(1\sigma_g)^2(2\delta_g)^2(\delta_u)^1(1\sigma_u)^1)]$ with T_e = 21 760 cm^{-1}, $^4\Pi_u(5)$ $[(\pi_u)^2(1\sigma_g 2\sigma_g)^4(\delta_g)^2(1\sigma_u)^1)]$ with T_e = 24 960 cm^{-1}, and $^4\Pi_u(6)$ $[(\pi_u)^3(1\sigma_g)^2(\delta_g)^2(\delta_u)^2)]$ with T_e = 26 836 cm^{-1}. Even if these numbers are higher than the result of the FOCI method and above our observed spectral region, it may provide evidence for the existence of the $X^4\Sigma_g^- \rightarrow {}^4\Pi_u$ transition(s) in the 16 000−18 000 cm^{-1} region when the effect of CI interactions is considered.

In doublet electronic configurations of the Nb_2^+, replacing the occupied orbital $\delta_g^1(\beta)$ with the unoccupied orbital $\delta_g^*(\beta)$ using the opt-TS methods produced a potential energy surface (PES) that lowered one of the $^2\Gamma_g$ and $^2\Sigma_g^+$ low-lying states as much as 2140 cm^{-1} at their minima. Because of the partially occupied $\delta_g(\alpha)$ and $\delta_g(\beta)$ molecular orbitals, the DFT calculations failed to determine which of the states has $^2\Gamma_g$ or $^2\Sigma_g^+$ symmetry. Therefore, the symmetry of the predicted lowest doublet energy level still remains ambiguous for us. However, Hund's rule tells us that the lowest doublet low-lying state should be the $^2\Gamma_g$ state instead the $^2\Sigma_g^+$ state. In such a case, we attempted to calculate the low-lying states $^2\Gamma_g$ and $^2\Sigma_g^+$ for V_2^+, $^2\Gamma$ and $^2\Sigma^+$ for the NbV^+, $^1\Gamma_g$ and $^1\Sigma_g^+$ for V_2 and Nb_2, and $^1\Gamma$ and $^1\Sigma^+$ for NbV dimer molecules, in order to compare with their experimentally known relative distances. As shown in Table 4, when comparing the calculated lowest $^2\Sigma_g^+$ low-lying state of V_2^+/NbV^+ and $^1\Sigma_g^+$ low-lying states of $V_2/Nb_2/NbV$ with their experimental values, it seems that the lowest doublet states of the $V_2^+/Nb_2^+/NbV^+$ dimer cations must have $^2\Gamma_g/^2\Gamma$symmetry and the lowest singlet energy levels of the $V_2/Nb_2/NbV$ neutral dimer molecules must possess $^1\Gamma_g/^1\Gamma$ symmetry. Therefore, we conclude that the lowest doublet state of the niobium dimer cation should be the $^2\Gamma_g$ state instead of the $^2\Sigma_g^+$ state.

III. Experimental Studies on Niobium Dimer Cation

A. Experimental Procedure. A brief outline of the experimental procedure is given here, as detailed descriptions can be found elsewhere.[26] The apparatus used in the present study is specifically designed for the study of the photofragmentation of isolated, internally cold, chemically bonded cluster ions. It consists of a three-stage differentially evacuated chamber, which contains a laser vaporization cluster ion source, a mass-selection section, which consists of a time-of-flight (TOF) mass spectrometer followed by a mass gate, and a tandem reflectron TOF mass spectrometer. The ion source has been developed for production of positively and negatively charged cluster species prior to supersonic expansion to minimize the internal excitation of the parent ions and, therefore, its effect on the photofragmentation process. A metal atom plasma is formed by pulsed laser vaporization of a Nb metal target rod (Goodfellow, 99.9%) mounted in a cluster source fixture. The second harmonic output (532 nm) of an Nd:YAG laser is used for this purpose, focusing a 20−35 mJ, 10 ns pulse duration onto the rod source with a lens. Crucial to the successful generation of a fairly intense beam of niobium cluster cation molecules was the continual ablation of the rod surface until the deeply penetrating layer of metal oxide had been largely removed. Vaporization was synchronized to the passage of the peak of a pulse of helium gas from a commercial molecular beam valve (120−140 psi backing pressure) over the target. The cluster concentration was augmented by allowing the gas mixture to pass through to the clustering channel, prior to supersonic expansion into vacuum and the first TOF stage. The selected niobium cluster cations (Nb_2^+) were thereafter fragmented by a Nd:YAG-pumped (532 nm), tunable-pulsed PDL dye laser (operating with Rhodamine 590, Coumarin 500, Coumarin 540A, DCM, Sulfarhodamine 640, Kiton Red 610, or Fluorescein 548) in the 15 500−18 500 cm^{-1} region. A tandem TOF mass spectrometer and reflectron have been constructed to monitor the dissociation caused by pulsed laser fragmention of the initially mass-selected cluster ions. This spectrometer is optimized to allow for maximum overlap of the ion and dissociation laser beams. In order to distinguish the parent and fragmented particles from each other, the reflectron acts as a second TOF spectrometer to separate the fragment and

TABLE 3: Calculated Doublet and Quartet Electronic Energy Levels of Nb_2^+ at TD-BLYP/LanL2DZ Level

sym	transition	configuration[a]	ω_e (cm^{-1})	R_e (Å)	T_e (cm^{-1})
$X^4\Sigma_g$		$(\pi_u)^4(1\sigma_g)^2(2\sigma_g)^1(\delta_g)^2$	436	2.121	0
$^2\Gamma_g$		$(\pi_u)^4(1\sigma_g)^2(2\sigma_g)^1(\delta^2_g(^1\Gamma_g))$	420	2.110	1 560
$^2\Sigma_g^-$		$(\pi_u)^4(1\sigma_g)^2$ $(\delta^2_g(^3\Sigma_g^-))x(2\sigma_g)^1$	420	2.110	2 080
$^2\Sigma_g^+$		$(\pi_u)^4(1\sigma_g)^2$ $(\delta^2_g(^1\Sigma_g^+))x(2\sigma_g)^1$	420	2.117	3 700
$^4\Sigma_g(2)$	$1\sigma_g\rightarrow2\sigma_g$	$(\pi_u)^4(1\sigma_g)^1(2\sigma_g)^2(\delta_g)^2$	500	2.220	4 500
$^2\Delta_g(1)$	$\delta_g\rightarrow2\sigma_g$	$(\pi_u)^4(1\sigma_g)^2(2\sigma_g)^2(\delta_g)^1$	440	2.095	6 200
$^4\Gamma_u$	$\delta_g\rightarrow\delta_u$	$(\pi_u)^4(1\sigma_g)^2(2\sigma_g)^1(\delta_g)^1(\delta_u)^1$	245	2.381	7 070
$^4\Delta_g$	$\sigma_g^1\rightarrow\delta_g$	$(\pi_u)^4(1\sigma_g2\sigma_g)^2(\delta_g)^3$	430	2.221	7 359
$^4\Pi_u(1)$	$\pi_u\rightarrow2\sigma_g$	$(\pi_u)^3(1\sigma_g)^2(2\sigma_g)^2(\delta_g)^2$	410	2.253	7 862
$^2\Sigma_g^-(2)$	$1\sigma_g\rightarrow2\sigma_g$	$(\pi_u)^4(1\sigma_g)^1(2\sigma_g)^2(\delta_g^2(^3\Sigma_g^-))$	450	2.252	8 500
$^4\Phi_u(1)$	$\pi_u\rightarrow\delta_g$	$(\pi_u)^3(1\sigma_g)^2(2\sigma_g)^1(\delta_g)^3$	335	2.234	9 980
$^2\Gamma_u$	$\delta_g\rightarrow\delta_u$	$(\pi_u)^4(1\sigma_g)^2(2\sigma_g)^1(\delta^1_g\delta^1_u)$	330	2.250	10 000
$^2\Pi_u(1)$	$\pi_u\rightarrow2\sigma_g$	$(\pi_u)^3(1\sigma_g)^2(2\sigma_g)^2(\delta_g^2(^3\Sigma_g^-))$	398	2.270	10 500
$^2\Delta_g(2)$	$\sigma_g\rightarrow\delta_g$	$(\pi_u)^4(1\sigma_g2\sigma_g)^2(\delta_g)^3$	430	2.165	10 900
$^4\Sigma_u(1)$	$\delta_g\rightarrow\delta_u$	$(\pi_u)^4(1\sigma_g2\sigma_g)^3(\delta_g)^1(\delta_u)^1$	305	2.295	11 100
$^4\Delta_u(1)$	$\sigma_g\rightarrow\delta_u$	$(\pi_u)^4(1\sigma_g2\sigma_g)^2(\delta_g)^2(\delta_u)^1$	280	2.117	11 410
$^4\Pi_u(2)$	$\pi_u\rightarrow\delta_g$	$(\pi_u)^3(1\sigma_g)^2(2\sigma_g)^1(\delta_g)^3$	360	2.238	12 920
$^4\Delta_u(2)$	$\sigma_g\rightarrow\delta_u$	$(\pi_u)^4(1\sigma_g2\sigma_g)^2(\delta_g)^2(\delta_u)^1$	334	2.335	13 435
$^4\Phi_g(1)$	$\pi_u\rightarrow\delta_u$	$(\pi_u)^3(1\sigma_g)^2(2\sigma_g)^1(\delta_g)^1(\delta_u)^1$	275	2.435	13 483
$^2\Phi_u(1)$	$\pi_u\rightarrow\delta_g$	$(\pi_u)^3(1\sigma_g)^2(2\sigma_g)^1(\delta_g)^3$	320	2.225	13 600
$^2\Sigma_u(1)$	$\delta_g\rightarrow\delta_u$	$(\pi_u)^4(2\sigma_g2\sigma_g)^3\delta_g\delta_u$	340	2.240	13 700
$^4\Pi_g(1)$	$\pi_u\rightarrow\delta_u$	$(\pi_u)^3(1\sigma_g)^2(2\sigma_g)^1(\delta_g)^2(1\delta_u)^1$	290	2.427	14 873
$^4\Sigma_u(2)$	$\sigma_g\rightarrow1\sigma_u$	$(\pi_u)^4(1\sigma_g2\sigma_g)^2(\delta_g)^2(1\sigma_u)^1$	335	2.390	15 000
$^2\Sigma_u(2)$	$\sigma_g\rightarrow\sigma_u$	$(\pi_u)^4(1\sigma_g2\sigma_g)^2(\delta_g(^3\Sigma_g^-))^2(1\sigma_u)^1$	300	2.310	15 000
$^2\Delta_u(1)$	$\sigma_g\rightarrow\delta_u$	$(\pi_u)^4(1\sigma_g2\sigma_g)^2(\delta_g)^2(\delta_u)^1$	300	2.265	15 300

[a] Each excited state results from more than one electronic isoconfigurational interaction, but only the dominant part of the isoelectronic configuration is provided here.

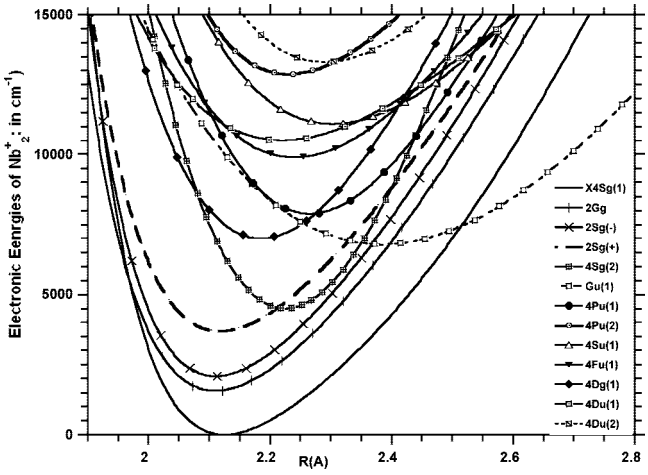

Figure 2. The calculated quartet and doublet energy levels of the Nb_2^+ at BLYP/LanL2DZ level of the DFT.

the parent in time. The resulting particles are then detected by a microchannel plate (MCP). Spectra are obtained by monitoring the intensity of a chosen fragment ion as a function of photofragmentation wavelength.

The desired cluster ions may be dissociated 1 μs after exit from the mass gate, through a field-free region by irradiation with the output of a Nd:YAG-pumped PDL dye laser.

B. One-Color Multiphoton Fragmentation. The resonant one-color three-photon dissociation spectrum of Nb_2^+ obtained by detection of the Nb^+ fragment ion as a function of incident photon energy was taken at a resolution of 1.3 cm^{-1} in the range of 16 000−18 450 cm^{-1}. We also attempted to obtain high-resolution spectra at many peak positions, but our laser resolution was not sufficient to obtain a well-resolved rotational spectrum. As shown in Figure 3, the dissociation spectrum of Nb_2^+ exhibited many well-resolved strong features that are centered around 16 127, 17 065, and 18 891 cm^{-1} and as many medium and weak features dispersed through the spectrum. These observed sharp peaks in the multiphoton fragmentation spectrum of Nb_2^+ may result from the bound−bound transition resonant enhancement of the multiphoton fragmentation of Nb_2^+ maximum at the absorption of the first photon in the one-color three-photon fragmentation. Furthermore, the spectrum explicitly involves multiple band structures and several heavily mixed overlapping transition. In most cases, sets of multiplet band structures can be distinguished with distinct progressions within each set, but in some cases, the intensity of some peaks dramatically decreases or disappears. For instance, in a comparison of the relatively intense peaks at 18 047, 18 063, and 18 082 cm^{-1} in the spectrum from Smalley et al.[27] to those in ours, they are very weak or almost disappear in our spectrum. A dramatic decrease in these peak intensities might be attributable to the resonance problem at the absorption of the first or second photon in the three-photon fragmentation. However, for the transition metals, because of the high density of the vibro-electronic states in the higher energies, the distance between discrete energy levels is expected to be very close, and these states are anticipated to appear as a continuous band with regard to the bandwidth of the excitation laser (the theoretical bandwidth of our fragmentation laser is about 0.07 cm^{-1}). This rules out the resonance problem at the absorption of the second photon. Thus, these observed peaks at 18 047, 18 063, and 18 082 cm^{-1} in the spectrum from Smalley et al.[27] may originate from another low-lying state, or they might be hot bands. However, especially the peak at 18 082 cm^{-1} joins a set of bands with a 365 cm^{-1} progression. As a consequence, based in part on our spectral assignment, we assume that the weaker or missing peaks within each subband might extensively suffer from the resonance problem at the absorption of the first photon.

Because of the complexity in the band structures and without high-resolution spectra, it is somewhat difficult to make an accurate assignment. Therefore, in the next section,

TABLE 4: Calculated Relative Distance between Singlet−Triplet and Quartet−Doublet Electronic Energy Levels of V_2/Nb_2/NV and V_2^+/Nb_2^+/NV^+

V_2 ($2S+1$)	wave function	ΔE (cm^{-1})	R (Å)	V_2^+ ($2S+1$)	wave function	ΔE (cm^{-1})	R (Å)
$X^3\Sigma_g^-$	$\psi_{12}(\alpha) = 0.80d_{-2}(\alpha) + 0.80d_{-2}(\alpha)$ $\psi_{13}(\alpha) = 0.80d_{+2}(\alpha) + 0.80d_{+2}(\alpha)$	0	1.791	$X^4\Sigma_g^-$	$\psi_{12}(\alpha) = 0.79d_{-2}(\alpha) + 0.79d_{-2}(\alpha)$ $\psi_{13}(\alpha) = 0.79d_{+2}(\alpha) + 0.79d_{+2}(\alpha)$	0	1.750
1	$\psi_{12}(\alpha) = 0.80d_{+2}(\alpha) + 0.80d_{+2}(\alpha)$ $\psi_{12}(\beta) = 0.80d_{-2}(\beta) + 0.80d_{-2}(\beta)$	456	1.791	2	$\psi_{12}(\alpha) = 0.79d_{-2}(\alpha) + 0.79d_{-2}(\alpha)$ $\psi_{12}(\beta) = 0.79d_{+2}(\beta) + 0.79d_{+2}(\beta)$	2032	1.752
1	$\psi_{13}(\alpha) = 0.80d_{-2}(\alpha) + 0.80d_{-2}(\alpha)$ $\psi_{13}(\beta) = 0.80d_{-2}(\beta) + 0.80d_{-2}(\beta)$	2876	1.791	2	$\psi_{12}(\alpha) = 0.79d_{+2}(\alpha) + 0.79d_{+2}(\alpha)$ $\psi_{12}(\alpha) = 0.79d_{-2}(\alpha) + 0.79d_{-2}(\alpha)$	3148	1.754
				2	$\psi_{12}(\alpha) = 0.79d_{-2}(\alpha) + 0.79d_{-2}(\alpha)$ $\psi_{12}(\beta) = 0.79d_{-2}(\beta) + 0.79d_{-2}(\beta)$	4596	1.752

NbV	wave function	ΔE (cm^{-1})	R (Å)	NbV^+	wave function	ΔE (cm^{-1})	R (Å)
$X^3\Sigma_g^-$	$\psi_{13}(\alpha) = 0.74d_{-2}(\alpha(Nb) + 0.83d_{-2}(\alpha)(V)$ $\psi_{14}(\alpha) = 0.74d_{+2}(\alpha(Nb) + 0.83d_{+2}(\alpha)(V)$	0	1.988	$X^4\Sigma_g^-$	$\psi_{12}(\alpha) = 0.71d_{-2}(\alpha(Nb) + 0.84d_{-2}(\alpha)(V)$ $\psi_{13}(\alpha) = 0.71d_{+2}(\alpha(Nb) + 0.84d_{+2}(\alpha)(V)$	0	1.943
1	$\psi_{13}(\alpha) = 0.76d_{-2}(\alpha(Nb) + 0.81d_{-2}(\alpha)(V)$ $\psi_{13}(\beta) = 0.76d_{-2}(\beta)(Nb) + 0.81d_{-2}(\beta)(V)$	2702	1.986	2	$\psi_{13}(\alpha) = 0.75d_{-2}(\alpha)(Nb) + 0.81d_{-2}(\alpha)(V)$ $\psi_{12}(\beta) = 0.71d_{+2}(\beta)(Nb) + 0.84d_{+2}(\beta)(V)$	1774	1.945
1	$\psi_{13}(\alpha) = 0.74d_{-2}(\alpha(Nb) + 0.81d_{-2}(\alpha)(V)$ $\psi_{13}(\beta) = 0.74d_{+2}(\beta)(Nb) + 0.81d_{+2}(\beta)(V)$	537	1.987	2	$\psi_{12}(\alpha) = 0.71d_{-2}(\alpha)(Nb) + 0.83d_{-2}(\alpha)(V)$ $\psi_{13}(\alpha) = 0.71d_{+2}(\alpha)(Nb) + 0.83d_{+2}(\alpha)(V)$	2462	1.947
				2	$\psi_{12}(\alpha) = 0.75d_{+2}(\alpha)(Nb) + 0.81d_{+2}(\alpha)(V)$ $\psi_{12}(\beta) = 0.71d_{+2}(\beta)(Nb) + 0.84d_{+2}(\beta)(V)$	4103	1.945

Nb^2	wave function	ΔE (cm^{-1})	R (Å)	Nb_2^+	wave function	ΔE (cm^{-1})	R (Å)
$X^3\Sigma_g^-$	$\psi_{13}(\alpha) = 0.76d_{+2}(\alpha) + 0.76d_{+2}(\alpha)$ $\psi_{14}(\alpha) = 0.76d_{-2}(\alpha) + 0.76d_{-2}(\alpha)$	0	2.157	$X^4\Sigma_g^-$	$\psi_{12}(\alpha) = 0.76d_{+2}(\alpha) + 0.76d_{+2}(\alpha)$ $\psi_{13}(\alpha) = 0.76d_{-2}(\alpha) + 0.76d_{-2}(\alpha)$	0	2.120
1	$\psi_{13}(\alpha) = 0.76d_{+2}(\alpha) + 0.76d_{+2}(\alpha)$ $\psi_{13}(\beta) = 0.76d_{+2}(\beta) + 0.76d_{+2}(\beta)$	2400	2.157	2	$\psi_{12}(\alpha) = 0.76d_{-2}(\alpha) + 0.76d_{-2}(\alpha)$ $\psi_{12}(\beta) = 0.76d_{+2}(\beta) + 0.76d_{+2}(\beta)$	1560	2.118
1	$\psi_{13}(\alpha) = 0.76d_{+2}(\alpha) + 0.76d_{+2}(\alpha)$ $\psi_{13}(\beta) = 0.76d_{-2}(\beta) + 0.76d_{-2}(\beta)$	560	2.157	2	$\psi_{12}(\alpha) = 0.76d_{+2}(\alpha) + 0.76d_{+2}(\alpha)$ $\psi_{12}(\alpha) = 0.76d_{-2}(\alpha) + 0.76d_{-2}(\alpha)$	2090	2.116
				2	$\psi_{13}(\alpha) = 0.76d_{+2}(\alpha) + 0.76d_{+2}(\alpha)$ $\psi_{12}(\beta) = 0.76d_{+2}(\beta) + 0.76d_{+2}(\beta)$	3700	2.119

we will estimate a plausible second-order and first-order spin−orbit coupling in the ground and excited electronic states before making a tentative assignment.

C. Second-Order Spin−Orbit (SO) Coupling in the $X^4\Sigma_{\Omega g}^-$ ($1\sigma_g^2\pi_u^4 2\sigma_g^1\delta_g^2$) Ground State. As mentioned earlier, an experimental value for the second-order spin−orbit splitting (Δ) has not yet been reported, except a few theoretical calculations: 142 cm^{-1} by Simard et al.;[29] 109, 119, and 166 cm^{-1} by Aydin et al.;[26] and 145 cm^{-1} from the INDO/S-SOCI calculations by O'Brien.[31] However, Balasubramanian and Zhu[30] have performed the FOCI at the CASSCF/MRCI level and they found 18 low-lying electronic states below 16 900 cm^{-1} and but no $^2\Sigma_{\Omega g}^+$ state found in this energy region. If the distance between the $X^4\Sigma_g^-$ ($...2\sigma_g^1\delta_g^2$) and $^2\Sigma_g^+$ ($...2\sigma_g^1\delta_g^2$) states is higher than 16 900 cm^{-1}, then, the value of Δ must be less than 40 cm^{-1}. However, this value seems too small given the trends in measured values of Δ for the V_2^+ ($\Delta = 20$[34] and 21[35] cm^{-1}) and VNb^+ ($\Delta = 82$[34] cm^{-1}),

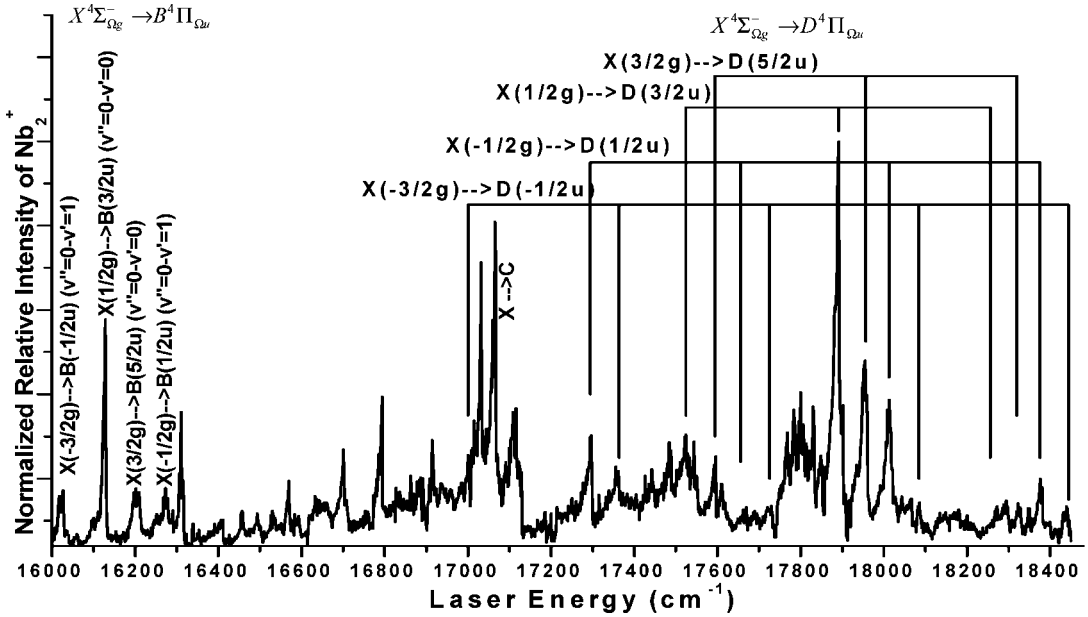

Figure 3. Resonant multiphoton fragmentation spectrum of Nb^{2+}. The strong peaks located around 16 120, 17 065, and 17 890 cm^{-1} are assigned to the $X^4\Sigma_g^- \rightarrow B^4\Pi_u$, $X^4\Sigma_g^- \rightarrow C^4\Pi_u$, and $X^4\Sigma_g^- \rightarrow D^4\Pi_u$ type transitions, respectively. The peaks at 17 033 (narrow) and 17 800 cm^{-1} may be candidates for $X^4\Sigma_{\Omega g}^- \rightarrow {}^4\Sigma_{\Omega u}^-$ transitions; see the text folr more detail.

which have the same ground-state symmetry, $X^4\Sigma_g^-$, resulting from the similar valence electronic configuration, $\pi_u^4 1\sigma_g^2 2\sigma_g^1 \delta_g^2$ (for V_2^+) and $\pi^4 1\sigma^2 2\sigma^1 \delta^2$ (for VNb^+).[31,34,35] In their neutral species, $\Delta = 75$ cm^{-1} for V_2,[36] 230 cm^{-1} for VNb,[34] and 410 cm^{-1} for Nb_2,[10,37] and these have $X^3\Sigma_g^-$/$X^3\Sigma^-$ ground state symmetry that results from the $\pi_u^4 1\sigma_g^2 2\sigma_g^2 1\delta_g^2$ ($\pi^4 1\sigma^2 2\sigma^2 1\delta^2$) valence electronic configuration.

Since these neutral and cationic dimer molecules, $Nb_2^{(0/+)}$, $V_2^{(0/+)}$, and $VNb^{(0/+)}$, have similar electronic configurations in their ground state, we may estimate a value for the second-order spin−orbit splitting (Δ) for Nb_2^+ by scaling the Δ values of the Nb_2^+ and Nb_2, $\Delta(Nb_2^+;X^4\Sigma_g^- - {}^2\Sigma_g^+)/\Delta(Nb_2;X^3\Sigma_g^- - {}^1\Sigma_g^+)$, to the corresponding splitting in the ground state of the V_2/V_2^+ and VNb/VNb^+ by the use of their measured values. We estimated two comparable Δ values for Nb_2^+ using eqs 1 and 2, $\Delta = 146$ and 142 cm^{-1}, which are consistent with DFT and INDO/S calculations.

$$Nb_2^+\Delta E(X^4\Sigma^-_{(\mp 3/2)g} - X^4\Sigma^-_{(\mp 1/2)g}) = Nb_2\Delta E(X^3\Sigma^-_{1g} - X^3\Sigma^-_{0g})\left[\frac{V_2^+\Delta E(X^4\Sigma^-_{(\mp 3/2)g} - X^4\Sigma^-_{(\mp 1/2)g})}{V_2\Delta E(X^3\Sigma^-_{1g} - X^3\Sigma^-_{0g})}\right] = 410\left[\frac{82}{230}\right] = 146\ \text{cm}^{-1} \quad (1)$$

$$Nb_2^+\Delta E(X^4\Sigma^-_{(\mp 3/2)g} - X^4\Sigma^-_{(\mp 1/2)g}) = Nb_2\Delta E(X^3\Sigma^-_{1g} - X^3\Sigma^-_{0g})\left[\frac{NbV^+\Delta E(X^4\Sigma^-_{(3/2)} - X^4\Sigma^-_{(1/2)})}{NbV\Delta E(X^3\Sigma^-_{1} - X^3\Sigma^-_{0})}\right] = 410\left[\frac{26}{75}\right] = 142\ \text{cm}^{-1} \quad (2)$$

Substituting these numbers ($\Delta = 142$ and 146 cm^{-1}) into eq 3 gives a value for the $E(^2\Sigma^+_{\pm 1/2g};\ldots 2\sigma_g^1\delta_g^2) = 4577$ and 4467 cm^{-1}, respectively.

$$E(^2\Sigma^+_{\pm 1/2g}) - E(X^4\Sigma^-_{\pm 1/2g}) = \frac{H_{12}^2 + 2\Delta^2}{\Delta} \quad (3)$$

where, $E(^2\Sigma^+_{\pm 1/2g}) = E^0(^2\Sigma^+_{\pm 1/2g}) + \Delta$, $E(X^4\Sigma^-_{\pm 1/2g}) = E^0(^4\Sigma^-_{\pm 1/2g}) - \Delta$ and $H_{12} = \langle X^4\Sigma^-_{\pm 1/2g}(1\sigma_2^2\pi_u^4 2\sigma_g^1\delta_g^2|H_{SO}|^2\Sigma^+_{\pm 1/2g}(1\sigma_2^2\pi_u^4 2\sigma_g^1\delta_g^2\rangle = 4/\sqrt{6}a_\delta(Nb_2^+)|X^4\Sigma^-_{(1/2)g}\rangle = 1/\sqrt{3}|\sigma_g\delta_g^+\delta_g^-(\alpha\alpha\beta + \alpha\beta\alpha + \beta\alpha\alpha)\rangle$ and $^2\Sigma^+_{(1/2)g}\rangle = 1/\sqrt{2}\sigma_g\delta_g^+\delta_g^-(\alpha\alpha\beta - \alpha\beta\alpha)\rangle$ are the relevant spin adapted Slater-type wave functions. The value of $a_\delta(Nb_2^+) = (\zeta_{4d}(Nb(^6D);5s^14d^4) + \zeta_{4d}(Nb^+(^5D);4d^4))/2 = 476$ cm^{-1} can be readily estimated from the averaged values of the atomic spin−orbit constants: $\zeta_{4d}(Nb(^6D)) = 448$ cm^{-1} and $\zeta_{4d}(Nb^+(^5D)) = 504$ cm^{-1}.

D. Excited State. As discussed earlier, Balasubramanian and Zhu[30] have calculated 18 low-lying states below 16 900 cm^{-1} for Nb_2^+ at the FOCI level. Their calculation showed that there are four $X^4\Sigma_g^- \rightarrow {}^4\Pi_u$ dipole-allowed electronic transitions, but only the two of the four $^4\Pi_u$ transitions lie in the observed spectral region of the Nb_2^+, henceforth termed as $A^4\Pi_u$ ($T_e = 16\,328$ cm^{-1}) and $B^4\Pi_u$ ($T_e = 16\,882$ cm^{-1}) states. Their major valence electronic configurations are respectively $1\sigma_g^1\pi_u^3 2\sigma_g^1\delta_g^4$ (21.7%) + $1\sigma_g^2\pi_u^3 2\sigma_g^1\delta_g^3$ (32.2%) and $1\sigma_g^1\pi_u^3 2\sigma_g^1\delta_g^4$ (31.0%) + $1\sigma_g^2\pi_u^3 2\sigma_g^1\delta_g^3$ (26.4%).[30] The spin-adapted Slater type wave functions for these excited states may be written in terms of a linear combination of these dominant open-shell configurations

$$A^4\Pi_{(5/2)u} = C|1\sigma_g 2\sigma_g\pi_u^-(\alpha\alpha\alpha)\rangle + \sqrt{1-C^2}|2\sigma_g\pi_u^-\delta_g^+\rangle \quad (3a)$$

$$A^4\Pi_{(3/2)u} = \frac{C}{\sqrt{3}}|1\sigma_g 2\sigma_g\pi_u^-(\alpha\alpha\beta + \alpha\beta\alpha + \beta\alpha\alpha)\rangle + \frac{\sqrt{1-C^2}}{\sqrt{3}}|2\sigma_g\pi_u^-\delta_g^+(\alpha\alpha\beta + \alpha\beta\alpha + \beta\alpha\alpha)\rangle \quad (3b)$$

$$A^4\Pi_{(1/2)u} = \frac{C}{\sqrt{3}}|1\sigma_g 2\sigma_g\pi_u^-(\alpha\beta\beta + \beta\alpha\beta + \beta\beta\alpha)\rangle + \frac{\sqrt{1-C^2}}{\sqrt{3}}|2\sigma_g\pi_u^-\delta_g^+(\alpha\beta\beta + \beta\alpha\beta + \beta\beta\alpha)\rangle \quad (3c)$$

$$A^4\Pi_{(-1/2)u} = C|1\sigma_g 2\sigma_g\pi_u^-(\beta\beta\beta)\rangle + \sqrt{1-C^2}|2\sigma_g\pi_u^-\delta_g^+\rangle \quad (3d)$$

where the C is the weight of a single electronic configuration that contributes to each $A^4\Pi_u$ and $B^4\Pi_u$ excited states and takes a value from zero to one, $0 \le C \le 1$.

The first-order spin−orbit coupling matrix element, $\langle^4\Pi_{\Omega u}|H_{SO}|^4\Pi_{\Omega u}\rangle = \Sigma\Lambda A$, for each electronic state can be expressed in terms of the atomic spin−orbit coupling constant

$$\langle A^4\Pi_{5/2}|\sum_i a_i l_i s_i|A^4\Pi_{5/2}\rangle = \frac{C^2 a_\pi(Nb_2^+)}{2} + (1-C^2)\left[\frac{2a_\delta(Nb_2^+) - a_\pi(Nb_2^+)}{2}\right] \quad (4a)$$

$$\langle A^4\Pi_{3/2}|\sum_i a_i l_i s_i|A^4\Pi_{3/2}\rangle = \frac{C^2 a_\pi(Nb_2^+)}{6} + (1-C^2)\left[\frac{2a_\delta(Nb_2^+) - a_\pi(Nb_2^+)}{6}\right] \quad (4b)$$

$$\langle A^4\Pi_{1/2}|\sum_i a_i l_i s_i|A^4\Pi_{1/2}\rangle = -\frac{C^2 a_\pi(Nb_2^+)}{6} + (1-C^2)\left[\frac{-2a_\delta(Nb_2^+) + a_\pi(Nb_2^+)}{6}\right] \quad (4c)$$

$$\langle A^4\Pi_{-1/2}|\sum_i a_i l_i s_i|A^4\Pi_{-1/2}\rangle = -\frac{C^2 a_\pi(Nb_2^+)}{2} + (1-C^2)\left[\frac{-2a_\delta(Nb_2^+) + a_\pi(Nb_2^+)}{2}\right] \quad (4d)$$

where a_i is the averaged atomic spin−orbit constant, $a_i(XY) = [\zeta_i(X) + \zeta_i(Y)]/2$. Similarly, the spin-adapted Slater-type wave functions and the matrix elements for the $B^4\Pi_u$ electronic state, $\langle B^4\Pi_{\Omega u}|\sum_i a_i l_i s_i|B^4\Pi_{\Omega u}\rangle$, can be written by just replacing C^2 with $(1 - C^2)$ in eqs 4a−4c). The first-order spin−orbit splitting between Ω and $(\Omega - 1)$ components of the $A^4\Pi_u$ and $B^4\Pi_u$ excited states may be predicted using the averaged atomic spin−orbit constants. So far we have acknowledged that a value for the spin−orbit constants $a_\pi(Nb_2^+;{}^4\Pi_u)$ for Nb_2^+ has not been

reported yet, but we can estimate a reasonable value for the $a_\pi(Nb_2^+;^4\Pi_u(\sigma_g\pi_u\delta_g))$ by scaling the value from the corresponding $A^4\Pi(V_2)$ state of the V_2:[36] taking the known spin−orbit parameters of $a_\delta(V_2;X^3\Sigma_g^-) = 145\ cm^{-1}$,[36] $a_\pi(V_2;A^3\Pi_u(\sigma_g\pi_u\delta_g)) = 210\ cm^{-1}$, and $a_\delta(Nb_2^+) = 476\ cm^{-1}$ using eq 5, we have

$$a_\pi(Nb_2^+;^4\Pi) = a_\pi(Nb_2;^3\Pi)\frac{a_\delta(Nb_2^+;X^4\Sigma_{\Omega g}^-)}{a_\delta(Nb_2;X^3\Sigma_{\Omega g}^-)}$$
$$= a_\pi(V_2;^3\Pi)\frac{a_\delta(Nb_2^+;X^4\Sigma_{\Omega g}^-)}{a_\delta(V_2;X^3\Sigma_{\Omega g}^-)} = 210\frac{476}{145} = 690\ cm^{-1} \quad (5)$$

By substituting the averaged values of the atomic spin−orbit constants into eqs 4a−4c, the splitting between Ω and (Ω − 1) components of the $A/B^4\Pi_{\Omega u}$ electronic states may be expressed in term of the parameter C (weigh of a single electronic configuration).

$$A^4\Pi_{\Omega u} - A^4\Pi_{(\Omega-1)u} = \frac{C^2}{3}[2a_\delta(Nb_2^+) - a_\pi(Nb_2^+)] + \frac{(1-C^2)}{3}[a_\pi(Nb_2^+] = 88C^2 + 230(1-C^2)\ cm^{-1} \quad (6)$$

$$B^4\Pi_{\Omega u} - B^4\Pi_{(\Omega-1)u} = \frac{(1-C^2)}{3}[2a_\delta(Nb_2^+) - a_\pi(Nb_2^+)] + \frac{C^2}{3}[a_\pi(Nb_2^+] = 88(1-C^2) + 230C^2\ cm^{-1} \quad (7)$$

For $C = 1$, eqs 6 and 7 may provide upper and lower limiting values for the average distance between Ω and (Ω−1) components of the $A/B^4\Pi_{\Omega u}$ electronic states:

$$A^4\Pi_{\Omega u} - A^4\Pi_{(\Omega-1)u} = 88\ cm^{-1} \quad \text{and} \quad B^4\Pi_{\Omega u} - B^4\Pi_{(\Omega-1)u} = 230\ cm^{-1}$$

When we attempted to assign the spectrum of the Nb_2^+ based on only two $X^4\Sigma_{\Omega g}^- \rightarrow A/B^4\Pi_{\Omega u}$ transitions by taking account of the estimated second-order splitting ($\Delta \sim 145\ cm^{-1}$) in the $X^4\Sigma_g^-$ ($...2\sigma_g^1\delta_g^2$) ground-state and the first-order coupling parameters $A/B^4\Pi_{\Omega u}$ excited states, we were not able to assign the strong features due to the large separation between the strong features centered around 16 127, 17 065, and 17 890 cm^{-1}. These separations are respectively about 1040 and 830 cm^{-1}. These large separations between the strong features indicate the existence of another $X^4\Sigma_{\Omega g}^- \rightarrow {}^4\Pi_{\Omega u}$ and/or $X^4\Sigma_{\Omega g}^- \rightarrow {}^4\Sigma_{\Omega u}^-$ transition. In fact, this experimental observation is not so surprising, due to the existence of many low-lying electronic states in the transition metals. These electronic states may be asymptotic to the second or third separated atomic limits as well as the lowest atomic limit. For instance, since $A^4\Pi_u$ and $B^4\Pi_u$ excited states are associated with the lowest atomic fragmentation limits of the Nb and Nb^+ atoms, $Nb(^6D,5s^14d^4) + Nb^+(^5D,4d^4)$, we would expect another two $^4\Pi_u$ states that may be associated with the second lowest atomic limit, $Nb(^4F,4d^35s^2) + Nb^+(^5D,4d^4)$, which lie only 1449 cm^{-1} (or 1486 cm^{-1}) (spin−orbit averaged) above the lowest energy limit (henceforth, referred to as $C^4\Pi_{(\Omega)u}$ and $D^4\Pi_{(\Omega)u}$ excited states). The total spin−orbit splitting in the $C^4\Pi_{(\Omega)u}$ and $D^4\Pi_{(\Omega)u}$ states may respectively be similar to the splitting in the $A^4\Pi_u$ and $B^4\Pi_u$ excited states, since they have similar open-shell electronic configuration. Also, the third lowest fragmentation limit, $Nb_2^+ \rightarrow Nb(^6D,4d^45s^1) + Nb^+(^4F,5s^14d^3)$, is not too far from the first dissociation energy limit, which lies about 2640 cm^{-1} (spin−orbit averaged) above the first one and about 1200 cm^{-1} above the second one.

Now, we will tentatively assign the observed spectrum of the Nb_2^+ by taking account of these estimated first-order and second-order spin−orbit splitting in the excited and ground states with the nonresonance problems for the peaks progressions within the subbands as discussed earlier.

E. Assignment of the Nb_2^+ Spectrum. The spectrum as seen in Figure 3, explicitly reveals three groups. The groups (from 1 to 3) seem to have an alternating intensity. In addition, some of the peaks are broader than the others, and the peaks were red degraded. This suggests that they are band heads and indicates the fact that $r_e' > r_e''$ and $\omega_e'' > \omega_e'$. A careful comparison of the bandwidths of the strong peaks at 16 125/17 032/17 065 cm^{-1} to the strong peaks at 17 890/17 958/18 013 cm^{-1} indicates that some hot bands may closely overlap with these bands (at 17 890/17 958/18 013 cm^{-1}).

Based in part on estimated first- and second-order spin orbit coupling parameters together with calculated dipole-allowed electronic transitions, several assignment schemes were tried using three possible vibrational progressions such as 295 ± 5, 365 ± 3, and 420 ± 5 cm^{-1}. Assignment of the subbands based on 295 ± 5 or/and 420 ± 5 cm^{-1} peak progressions within each subband failed to explain most of the strong features. However, the band progression with 365 ± 3 cm^{-1} within each subbands almost explains most of the important strong features. In fact, the vibrational progression with 295 ± 5 or/and 420 ± 5 cm^{-1} develops from the combination of the relative distance (65 ± 5 cm^{-1}) between the nearby peaks and the 365 ± 3 cm^{-1} vibrational progression, for instance 365(3) ± 65(5) cm^{-1}. We can then partially assign the spectrum taking account of the vibrational progression of 365 ± 3 cm^{-1} and estimated second-order spin−orbit coupling (145 cm^{-1}) between the $X^4\Sigma_g^-$ ($...2\sigma_g^1\delta_g^2$) and $^2\Sigma_g^+$ ($...2\sigma_g^1\delta_g^2$) states, together with the lower and upper limiting values for the first-order spin−orbit coupling in the $^4\Pi_{\Omega u}$ excited states (88 and 231 cm^{-1}).

The distance between an averaged value of the observed peaks at 15 905/16 125 and 16 202 cm^{-1} (group B) and the averaged value of the peaks observed at 17 294/17 525 and 17 597 cm^{-1} (group D) are 1395 ± 5 cm^{-1}, nicely in accord with the spin−orbit averaged value of 1446 [38] or 1486 cm^{-1} [39] between the dissociation of the Nb_2^+ to its first-lowest ($Nb(^6D; ...5s^14d^4) + Nb^+(^5D; ...4d^4)$) and second-lowest ($Nb(^4F; ...5s^14d^4) + Nb^+(^5D; ...4d^4)$) atomic limits. Furthermore, they possess an analogous vibrational progression (365 ± 3 cm^{-1}). For that reason, we concluded that the observed features around 16 127 cm^{-1} in group B and around 17 297 cm^{-1} in group D result from the similar open-shell electronic configurations, but they are asymptotic to the lowest and the second lowest atomic limits, respectively. Thus, we assigned the peaks at 16 020, 15 910, 16 127, and 16 202 cm^{-1} to $X^4\Sigma_{(-3/2)g}^- \rightarrow B^4\Pi_{(-1/2)u}(0-1)$, $X^4\Sigma_{(-1/2)g}^- \rightarrow B^4\Pi_{(1/2)u}(0-0)$, $X^4\Sigma_{(1/2)g}^- \rightarrow B^4\Pi_{(3/2)u}(0-0)$, and $X^4\Sigma_{(3/2)g}^- \rightarrow B^4\Pi_{(5/2)u}(0-0)$ transitions, respectively. The subbands beginning from 17 000/17 294/17 525 and 17 597 cm^{-1} are respectively attributed to $X^4\Sigma_{(-3/2)g}^- \rightarrow D^4\Pi_{(-1/2)u}(0-0)$, $X^4\Sigma_{(-1/2)g}^- \rightarrow D^4\Pi_{(1/2)u}(0-0)$, $X^4\Sigma_{(1/2)g}^- \rightarrow D^4\Pi_{(3/2)u}(0-0)$, and $X^4\Sigma_{(3/2)g}^- \rightarrow D^4\Pi_{(5/2)u}(0-0)$ transitions with the selection rules $\Delta\Sigma = 0$ and $\Delta\Lambda = \pm 1$. Here it should be noted that the $X^4\Sigma_{(-3/2)g}^- \rightarrow B^4\Pi_{(-1/2)u}(0-0)$ transition was not observed because one-color multiphoton fragmentation process changes from a three-photon process to four-photon process, as reported in our previous work.[25]

TABLE 5: Assigned Multiphoton Spectrum of the Nb_2^+

ν (cm^{-1})	peak intensity	assignment	ν (cm^{-1})	peak intensity	assignment
15 710	weak	D(3/2)−X(1/2),(0−1)	17 362	medium	D(−1/2)−X(−3/2),(1−0)
785	weak	D(5/2)−X(3/2),(0−1)	486	medium	D(5/2)−X(−3/2),(2−2)
910	weak	D(1/2)−X(−1/2),(0−0)	525	medium	D(3/2)−X(1/2),(0−0)
16 022	medium	D(−1/2)−X(−3/2),(1−0)	544	medium	D(5/2)−X(−3/2),(1−1)
28	medium	D(3/2)−X(1/2),(3−2)	592	medium	D(5/2)−X(−3/2),(0−0)
98	weak	D(5/2)−X(3/2),(2−2)	597	medium	D(1/2)−X(−1/2),(2−1)
127	strong	D(3/2)−X(1/2),(0−0)	605	weak	
202	medium	D(5/2)−X(3/2),(0−0)	768	medium	D(3/2)−X(1/2),(3−2)
275	medium	D(1/2)−X(−1/2),(1−0)	784	medium	
310	?		800	medium	
408	weak	D(5/2)−X(3/2),(3−3)	813	weak	
458	weak	D(5/2)−X(3/2),(3−2)	832		D(3/2)−X(1/2),(2−1)
498	weak	D(3/2)−X(1/2),(1−0)	850	medium	D(5/2)−X(−3/2),(3−2)
530	weak	D(−1/2)−X(−3/2),(1−2)	891	strong	D(3/2)−X(1/2),(1−0)
568	medium	D(5/2)−X(3/2),(1−0)	902	medium	D(5/2)−X(−3/2),(2−1)
583	weak	D(−1/2)−X(−3/2),(0−1)	934	medium	
700	medium		958	strong	D(5/2)−X(−3/2),(1−0)
794	?		962	overlap	D(1/2)−X(−1/2),(3−1)
878	weak	D(1/2)−X(−1/2),(0−1)	18 005	overlap	
914	weak		15	strong	D(1/2)−X(−1/2),(1−0)
936	weak	D(−1/2)−X(−3/2),(1−1)	26	weak	D(−1/2)−X(−3/2),(4−1)
17 000	medium	D(−1/2)−X(−3/2),(0−0)	44		
33	strong		65	weak	
65	strong		84	weak	D(−1/2)−X(−3/2),(3−0)
108	medium	D(3/2)−X(1/2),(0−1)	298	weak	
115	medium		320	weak	D(5/2)−X(−3/2),(2−0)
178	weak	D(5/2)−X(−3/2),(0−1)	378	medium	D(1/2)−X(−1/2),(2−0)
296	strong	D(1/2)−X(−1/2),(0−0)	442	medium	D(−1/2)−X(−3/2),(4−0)

The measured distance between the components of $B^4\Pi_{\Omega u}$ excited-state as follows:

$$B^4\Pi_{(-1/2)u}(\nu' = 1) - B^4\Pi_{(1/2)u}(\nu' = 1) = 255 \pm 5\ cm^{-1}$$

$$B^4\Pi_{(3/2)u} - B^4\Pi_{(1/2)u} = 220 \pm 5\ cm^{-1}$$

$$B^4\Pi_{(5/2)u} - B^4\Pi_{(3/2)u} = 70 \pm 5\ cm^{-1}$$

$$B^4\Pi_{(5/2)u}(\nu' = 1) - B^4\Pi_{(-1/2)u}(\nu' = 1) = 550 \pm 5\ cm^{-1}$$

The measured total spin−orbit splitting between (Ω= −1/2u, $\nu' = 1$) and ($\Omega = 5/2u$, $\nu' = 1$) components of the $B^4\Pi_{\Omega u}$ state is about 550 cm^{-1}. This value gives an averaged value for the molecular spin−orbit constant (A_{SO}) for $B^4\Pi_{\Omega u}$ excited state: $A_{SO} = B^4\Pi_{\Omega u}(\nu' = 1) - B^4\Pi_{(\Omega-1)u}(\nu' = 1) \approx 183\ cm^{-1}$. For the $D^4\Pi_{\Omega u}$ excited state,

$$D^4\Pi_{(-1/2)u} - D^4\Pi_{(1/2)u} = 295 \pm 5\ cm^{-1}$$

$$D^4\Pi_{(3/2)u} - D^4\Pi_{(1/2)u} = 230 \pm 3\ cm^{-1}$$

$$D^4\Pi_{(5/2)u} - D^4\Pi_{(3/2)u} = 70 \pm 3\ cm^{-1}$$

$$D^4\Pi_{(5/2)u} - D^4\Pi_{(-1/2)u} = 597 \pm 3\ cm^{-1}$$

The total spin−orbit splitting between D($\Omega = 5/2u$) and D(Ω = −1/2u) is about 600 cm^{-1} and the averaged molecular spin−orbit constant $A_{SO} = D^4\Pi_{\Omega u}(\nu' = 0) - D^4\Pi_{(\Omega-1)u}(\nu' = 0) \cong 200\ cm^{-1}$. However, the distance between the D($\Omega = 1/2u$) and D(3/2u) bands is ∼ 230 cm^{-1}. This number suggests that there might be a vibrational interaction and/or a weak second-order spin−orbit interaction between $^4\Pi_u$ and $^2\Pi_u$ states that causes a red shift in the $\Omega = 1/2$ and 3/2 subbands by as much as 40 and 15 cm^{-1}, respectively, where the $^2\Pi_u$ state must lie above the $^4\Pi_u$ state. These shifts also exist in $\Omega = 1/2$ and 3/2 components of the $B^4\Pi_{(\Omega)u}$ state. As mentioned earlier, a matrix-isolated electron spin resonance (ESR) spectrum of Nb_2^+ (by Van Zee, Li, and Weltner[28]) indicates that the $^2\Pi_{(\Omega)u}$ states might be about 20 000 cm^{-1} above the $^2\Sigma^+_{\Omega g}$ ($...1\sigma_g^2\pi_u^4 2\sigma_g^1\delta_g^2$), although they recommended the $^2\Sigma^+_{\Omega g}$ ($...1\sigma_g^2\pi_u^4 2\sigma_g^1\delta_g^2$) as a ground state. This is in harmony with the observed red shift in the $\Omega = 1/2$ and 3/2 components of $^4\Pi_u$ excited states in our experiment. From these subband placements, we determined the second-order spin−orbit coupling (Δ) in the ground-state to be 145 cm^{-1}, in excellent agreement with values of 142 and 145 cm^{-1} estimated from eqs 1 and 2 as well as the DFT[26,29] and INDO/S-SOCI calculations.[31]

There are several peaks with relatively low intensity that might be fit to transitions to excited states from vibrationaly excited ground-state as hot bands. For instance, a set of subbands with a 365 ± 5 cm^{-1} vibrational progression, which originate from 17 108 (17 115) cm^{-1}, associate with (Ω = 3/2u) components of the $D^4\Pi_{(\Omega)u}$state with the ground-state vibrational frequency (ω_e'') of 420 ± 3 cm^{-1}. Another two peaks at 17 544 and 17 902 cm^{-1} may be fitted to a transition from X($\Omega = 3/2$ g)($\nu'' = 1$) to ($\Omega = 3/2u$)(ν') components of $D^4\Pi_{\Omega u}$ excited state. The peaks (relatively weak) at 17 768 and 17 850 cm^{-1} may be respectively attributed to transitions from X($\Omega = 1/2$g and 3/2g)($\nu'' = 2$) to ($\Omega = 3/2$u and 5/2u)(ν'). These fittings provide a value of 420 ± 3 cm^{-1} for the ground-state vibrational frequency (ω'') of Nb_2^+, which is compatible with the theoretical predictions such as $\omega'' = 420$, 430, 444 cm^{-1} at the different levels of the DFT calculations[26] and 430 cm^{-1} at the FOCI level.[30] A full assignment of the multiphoton fragmentation spectrum of the Nb_2^+ is given in Table 5. Table 6 shows the

TABLE 6: Determined Spectroscopic Parameters of Nb_2^+

	X	⟨B⟩	⟨D⟩
T_e (cm^{-1})	0	15 930	17 300
ω_e (cm^{-1})	418 ± 3	364 ± 3	364 ± 3
A_{SO} (cm^{-1})		∼183	∼200
Δ (cm^{-1})	145 ± 3		
$^2\Sigma_g^+ - X^4\Sigma_g^-$ (cm^{-1})	4400−4230[a]		

[a] $E(^2\Sigma^+_{\pm 1/2g}) - E(X^4\Sigma^-_{\pm 1/2g}) = (H_{12}^2 + 2\Delta^2)/\Delta$ and $H_{12} = \langle X^4\Sigma^-_{\pm 1/2g}(1\sigma_2^2\pi_u^4 2\sigma_g^1\delta_g^2 | H_{SO} | {}^2\Sigma^+_{\pm 1/2g}(1\sigma_2^2\pi_u^4 2\sigma_g^1\delta_g^2\rangle = 4/\sqrt{6}a_\delta(Nb_2^+)$.

measured spectroscopic constants of the ground and excited states of Nb_2^+.

Since the contributions from each dominant open-shell electronic configurations ($1\sigma_g^2\pi_u^3 2\sigma_g^1\delta_g^3$ and $1\sigma_g^1\pi_u^3 2\sigma_g^1\delta_g^4$) to each $B^4\Pi_{(\Omega)u}$ and $D^4\Pi_{(\Omega)u}$ state are roughly the same, then we can obtain a value for the $a_\delta(Nb,^4F,5s^24d^3)$ from eq 8 using the total spin−orbit splitting in the $B^4\Pi_{(\Omega)u}$ and $D^4\Pi_{(\Omega)u}$ states (that are respectively asymptote to the lowest and second lowest fragmentation limit) and atomic spin−orbit constants of the $Nb(^6D,5s^14d^4)$ and $Nb^+(^5D,4d^4)$. Substituting these numbers ($B^4\Pi_{(\Omega)u}$ = 550 ± 5 cm^{-1}, $D^4\Pi_{(\Omega)u}$ = 600 ± 3 cm^{-1}, $a_\delta(Nb;^6D,5s^14d^4) = 448\ cm^{-1}$ and $a_\delta(Nb^+;^5D,4d^4) = 504\ cm^{-1}$) into eq 8

$$\frac{(a_\delta(Nb;^4F) + a_\delta(Nb^+;^5D)}{(a_\delta(Nb;^6D) + a_\delta(Nb^+;^5D))} \approx \frac{(a_\pi(Nb;^4F) + a_\pi(Nb^+;^5D)}{(a_\pi(Nb;^6D) + a_\pi(Nb^+;^5D))} \approx \left(\frac{D^4\Pi_{5/2u} - D^4\Pi_{-1/2u}}{B^4\Pi_{5/2u} - B^4\Pi_{-1/2u}}\right) \quad (8)$$

then, we have

$$a_\delta(Nb;^4F) = (504 + 448)\left(\frac{600 \pm 3}{550 \pm 5}\right) - 504 = 535 \pm 15\ cm^{-1}$$

This number is in agreement with the reported value of $a_\delta(Nb;5s^24d^3,^4F) = 515 \pm 35\ cm^{-1}$ by Simard et al.[39] and provides evidence for the accuracy of our tentative assignment.

There are a few unassigned peaks left, such as two strong peaks at 17 032 cm^{-1} (narrow) and 17 065 cm^{-1} (red degraded) in group C and peaks at 17 784/17 800 cm^{-1} with medium intensity, which do not have vibrational progressions. The exception is a peak with relatively low intensity at 16 700 cm^{-1}, which can be the origin of the peak either at 17 033 or 17 065 cm^{-1} with vibrational progression 332 and 365 cm^{-1}, respectively. The calculations, at TD-BLYP/LanL2DZ level of the DFT, produced three dipole-allowed $X^4\Sigma^-_{\Omega g} \rightarrow {}^4\Sigma^-_{\Omega u}$ transitions at 16 000 cm^{-1}, with R_e = 2.196 Å and $\omega_e' = 360\ cm^{-1}$; at 17 900 cm^{-1}, with R_e = 2.483 Å and $\omega_e' = 315\ cm^{-1}$; and at 17 990 cm^{-1}, with R_e = 2.155 Å and $\omega_e' = 450\ cm^{-1}$. When the rotational structure is taken into account in case a, the band shape in $X^4\Sigma^-_{\Omega g} \rightarrow {}^4\Sigma^-_{\Omega u}$ is expected to show that the Q-branch dominates the others. In the $X^4\Sigma^-_{\Omega g} \rightarrow {}^4\Pi_{\Omega u}$, the R-branch is dominant and red degraded due to the band-head. Thus, owing to the very narrow band structure of the peaks at 17 033 and 17 800 cm^{-1}, these peaks may be candidates for $X^4\Sigma^-_{\Omega g} \rightarrow {}^4\Sigma^-_{\Omega u}$ transitions. The peak at the 17 065 cm^{-1} may be another $X^4\Sigma^-_{\Omega g} \rightarrow {}^4\Pi_{\Omega u}$ transition.

IV. Conclusion

The gas-phase electronic spectrum of the niobium dimer cation molecule was obtained with a laser vaporization−supersonic exposition source. A number of intense band systems centered around 16 127, 17 065 and 17 891 cm^{-1}, termed as B, C, and D transitions, respectively, were observed in the 16 000−18 450 cm^{-1} region and assigned as transitions from Ω = ±1/2 and ±3/2 spin−orbit components of $X^4\Sigma_g^-$ $(...2\sigma_g^1\delta_g^2)$electronic ground-state to Ω = ±1/2, 3/2, and 5/2 spin−orbit components of $B/C/D^4\Pi_u$ excited states. The spin−orbit averaged distance between the $B^4\Pi_{\Omega u}$ and $D^4\Pi_{\Omega u}$ excited states is about 1395 ± 5 cm^{-1}, which is nicely in accord with the spin−orbit averaged value of 1446 cm^{-1} between the dissociation of the Nb_2^+ to its first-lowest [$Nb(^6D; ...5s^14d^4) + Nb^+(^5D; ...4d^4)$] and second-lowest [$Nb(^4F; ...5s^14d^4) + Nb^+(^5D; ...4d^4)$] atomic limits. For that reason, we concluded that the observed features in group B and in group D result from the similar open-shell electronic configurations, but they are asymptotic to the lowest and the second-lowest atomic limits, respectively. The measured total spin−orbit splitting between (Ω = −1/2u, $\nu' = 1$) and (Ω = 5/2u, $\nu' = 1$) components of the $B^4\Pi_{\Omega u}$ state is ∼550 cm^{-1}. The total spin−orbit splitting between D(Ω = 5/2u,$\nu' = 0$) and D(Ω = −1/2u,$\nu' = 0$) is about 600 cm^{-1}. This value gives an averaged value for the molecular spin−orbit constant (A_{SO}) for $B^4\Pi_{\Omega u}$ and $D^4\Pi_{\Omega u}$ excited states: $A_{SO}(B^4\Pi_{\Omega u}(\nu' = 1)) \approx 183\ cm^{-1}$ and $A_{SO}(D^4\Pi_{\Omega u}(\nu' = 0)) \cong 200\ cm^{-1}$. From the placement of these subbands, we determined the second-order spin−orbit coupling (Δ) in the ground-state to be 145 cm^{-1}, in excellent agreement with values of 142 and 145 cm^{-1} estimated from eqs 1 and 2 as well as the DFT[26,29] and INDO/S-SOCI calculations.[31] From the fitting of several relatively weak transitions to excited states from vibrationaly excited ground state, we determined ground-state vibrational frequency (ω'') of Nb_2^+ to be 420 ± 3 cm^{-1}, which is compatible with the theoretical predictions: $\omega'' = 436\ cm^{-1}$ at the BLYP/LanL2DZ level and 430 cm^{-1} at the FOCI level.[30] On the basis of part of our tentative assignment and assuming that the contributions from each dominant open-shell electronic configurations ($1\sigma_g^2\pi_u^3 2\sigma_g^1\delta_g^3$ and $1\sigma_g^1\pi_u^3 2\sigma_g^1\delta_g^4$) to each $B^4\Pi_{(\Omega)u}$ and $D^4\Pi_{(\Omega)u}$ state are roughly the same, we also obtained a value of 535 ± 15 cm^{-1} for the atomic spin−orbit constant $a_\delta(Nb;^4F(5s^24d^3))$ using eq 8, which is compatible with the reported value of 515 ± 35 cm^{-1} by Simard et al.[39] and provides evidence for the accuracy of our tentative assignment.

There are a few unassigned peaks left, such as two strong peaks at 17 032 cm^{-1} (narrow) and 17 065 cm^{-1} (red degraded) in group C and peaks at 17 784/17 800 cm^{-1} with medium intensity, which do not have an explicit vibrational progression. On the basis of part of the TD-DFT calculations, the peaks at 17 033 and 17 800 cm^{-1} may be candidates for $X^4\Sigma^-_{\Omega g} \rightarrow {}^4\Sigma^-_{\Omega u}$ transitions and the peak at 17 065 cm^{-1} possibly results from another $X^4\Sigma^-_{\Omega g} \rightarrow {}^4\Pi_{\Omega u}$ transition; see the text for detail. The calculations also indicated that the most favorable next low-lying state is the $^2\Gamma_{\Omega g}$ $[...\delta_g^2(^1\Gamma_g)\otimes 2\sigma_g(\alpha)]$ symmetry, which lies only 1560 cm^{-1} above the ground state $X^4\Sigma_g^-$. Furthermore, the calculated ground-state spectroscopic properties from the first-row through the third-row transition metals are well correlated with their experimental results.

Acknowledgment. We wish to thank Prof. Joseph G. Eaton, Dr. Wumin Wang, and Dr. Shelley B. Deosaran for their assistance and suggestions in this work. This work was supported by the National Science Foundation, under Cooperative Agreement No. RII-9353488 and Grant No. CHE-0091362,

and by the City University of New York PSC-BHE Faculty Research Award Program and Center for Analysis of Structure and Interfaces (CASI).

Note Added after ASAP Publication. A correction was made to Table 1, footnote *a*. This manuscript was originally published on the Web on February 19, 2009. The corrected version was reposted on February 26, 2009.

References and Notes

(1) (a) Zheng, L.-S.; Brucat, P. J.; Pettiette, C. L.; Yang, S.; Smalley, R. E. *J. Chem. Phys.* **1985**, *83*, 4273. (b) Hopkins, J. B.; Langridge-Smith, P. R. R.; Morse, M. D.; Smalley, R. E. *J. Chem. Phys.* **1983**, *78*, 1627. (c) Langridge-Smith, P. R. R.; Morse, M. D.; Hansen, G. P.; Smalley, R. E.; Merer, A. J. *J. Chem. Phys.* **1984**, *80*, 593. (d) Elkind, J. L.; Weiss, F. D.; Alford, J. M.; Laaksonen, R. T.; Smalley, R. E. *J. Chem. Phys.* **1988**, *88*, 5215. (e) Heath, J. R.; Liu, Y.; O'Brien, S. C.; Zhang, Q.-L.; Curl, R. F.; Tittel, F. K.; Smalley, R. E. *J. Chem. Phys.* **1985**, *83*, 5520.

(2) (a) Sickafoose, S. M.; Langenberg, J. D.; Morse, M. D. J. *Phys. Chem. A* **2000**, *104*, 3521. (b) Taylor, S.; Spain, E. M.; Morse, M. D. *J. Chem. Phys.* **1990**, *92*, 2710. (c) Fu, Z.; Russon, L. M.; Morse, M. D.; Armentrout, P. B. *Int. J. Mass Spectrom.* **2001**, *204* (1/3), 143. (d) Fabbi, J. C.; Karlsson, L.; Langenberg, J. D.; Costello, Q. D.; Morse, M. D. *J. Chem. Phys.* **2003**, *118*, 9247. (e) Doverstal, M.; Lindgren, B.; Sassenberg, U.; Arrington, C. A.; Morse, M. D. *J. Chem. Phys.* **1992**, *97*, 7087. (f) Brugh, D. J.; Morse, M. D. *J. Chem. Phys.* **2002**, *117*, 10703. (g) Airola, M. B.; Morse, M. D. *J. Chem. Phys.* **2002**, *116*, 1313. (h) Lindholm, N. F.; Brugh, D. J.; Rothschopf, G. K.; Sickafoose, S. M.; Morse, M. D. *J. Chem. Phys.* **2003**, *118*, 2190. (i) Arrington, C. A.; Blume, T.; Doverstål, M.; Morse, M. D.; Sassenberg, U. *J. Phys. Chem.* **1994**, *98*, 1398. (j) Shin, S.; Brugh, D. J.; Morse, M. D. *Astrophys. J.* **2005**, *619*, 407. (k) Martinez, A.; Morse, M. D. *J. Chem. Phys.* **2006**, *124*, 124316. Ding, H.; Morse, M. D.; Apetrei, C.; Chacaga, L.; Maier, J. P. *J. Chem. Phys.* **2006**, *125*, 194315. (l) Rothschopf, G. K.; Morse, M. D. *J. Phys. Chem. A.* **2005**, *109*, 11358.

(3) (a) James, A. M.; Kowalczyk, P.; Simard, B. *Chem. Phys. Lett.* **1993**, *216*, 512. (b) James, A. M.; Kowalczyk, P.; Langlois, E.; Campbell, M. D.; Ogawa, A.; Simard, B. *J. Chem. Phys.* **1994**, *101*, 4485. (c) James, A. M.; Kowalczyk, P.; Simard, B. *J. Mol. Spectrosc.* **1994**, *164*, 260.

(4) (a) Song, L.; Eychmuller, A.; El-Sayed, M. A. *J. Phys. Chem.* **1988**, *92*, 1005. (b) Song, L.; Eychmuller, A.; Pierre, R. J. St.; El-Sayed, M. A. *J. Phys. Chem.* **1989**, *93*, 2485.

(5) (a) Loh, S. K.; Hales, D. A.; Lian, L.; Armentrout, P. B. *J. Chem. Phys.* **1989**, *90*, 5466. (b) Lian, L.; Su, C.-X.; Armentrout, P. B. *J. Chem. Phys.* **1992**, *97*, 4084. (c) Su, C. X.; Armentrout, P. B. *J. Chem. Phys.* **1993**, *99*, 6506. (d) Su, C. X.; Hales, D. A.; Armentrout, P. B. *J. Chem. Phys.* **1993**, *99*, 6613. (e) Hales, D. A.; Su, C.-X.; Lian, L.; Armentrout, P. B. *J. Chem. Phys.* **1994**, *100*, 1049.

(6) Ding, L. N.; Young, M. A.; Kleiber, P. D.; Stwalley, W. D. *J. Phys. Chem.* **1993**, *97*, 2181.

(7) Yang, D. S.; Hackett, P. A. J. *Electron Spectrosc. Relat. Phenom.* **2000**, *106* (2−3), 153.

(8) Li, R.; Balfour, W. J. *Chem. Phys. Lett.* **2005**, *403*, 102.

(9) Kagawa, T.; Aikawa, K.; Sato, F.; Kato, Y.; Iida, T. *Radiat. Prot. Dosim.* **2006**, *122* (1−4), 95.

(10) James, A. M.; Kowalczyk, P.; Fournier, R.; Simard, B. *J. Chem. Phys.* **1993**, *99*, 8504.

(11) Rixon, S. J.; Chowdhury, P. K.; Merer, A. J. *J. Mol. Spectrosc.* **2004**, *228*, 554.

(12) Fielicke, A.; Ratsch, C.; Helden, G. von.; Meijer, G. J. *Chem. Phys.* **2007**, *127*, 234306.

(13) Veldeman, N.; Janssens, E.; Hansen, K.; Haeck, J. De.; Silverans, R. E.; Lievens, P. *Faraday Discuss.* **2008**, *138*, 147.

(14) Calaminici, P.; Mejia-Olvera, R. *Comput. Lett.* **2007**, *3* (2−4), 201.

(15) Varshni, Y. P. *Chem. Phys.* **2007**, *342*, 297.

(16) Wu, Z. J. *Chem. Phys. Lett.* **2004**, *251*, 24.

(17) Zakin, M. R.; Brickman, R. O.; Cox, D. M.; Kaldor, A. *J. Chem. Phys.* **1988**, *88*, 3555.

(18) Hild, U.; Dietrich, G.; Kruckeberg, S.; Lindinger, M.; Luckenkirchen, K.; Schweikhard, L.; Walther, C.; Ziegler, J. *Phys. Rev. A.* **1998**, *57*, 2786.

(19) Ervin, K. M. *Chem. Rev.* **2001**, *101*, 391.

(20) Cox, D. M.; Reichmann, K. C.; Trevor, D. J.; Kaldor, A. *J. Chem. Phys.* **1988**, *88*, 111.

(21) Ball, K. D.; Berry, R. S.; Kunz, R. E.; Li, F. Y.; Wales, D. J. *Science* **1996**, *271*, 963.

(22) Loh, S. K.; Lian, L.; Armentrout, P. B. *J. Am. Chem. Soc.* **1989**, *111*, 3167.

(23) Hales, D. A.; Lian, L.; Armentrout, P. B. *Int. J. Mass Spectrom. Ion 346 Process.* **1990**, *102*, 269.

(24) Lombardi, J. R.; Davis, B. *Chem. Rev.* **2002**, *102*, 2431.

(25) Aydin, M.; Lombardi, J. R. *Int. J. Mass Spectrom.* **2004**, *235*, 91.

(26) Aydin, M. PhD dissertation, The City University of New York, New York, 2001.

(27) Brucat, P. J.; Zheng, L.-S.; Pettiette, C. L.; Yang, S.; Smalley, R. E. *J. Chem. Phys.* **1986**, *84*, 3078.

(28) Van Zee, R. J.; Li, S.; Weltner, W., Jr. *Chem. Phys. Lett.* **1994**, *217*, 381.

(29) Simard, B.; James, A. M.; Kowalczyk, P.; Fournier, R.; Hackett, P. A. *Proc. SPIE* **1994**, *376*, 2124.

(30) Balasubramanian, K.; Zhu, X. L. *J. Chem. Phys.* **2001**, *114*, 10375.

(31) O'Brien, T. A. *J. Phys. Chem. A.* **2004**, *108*, 5016.

(32) Pauling, L. *The Nature of the Chemical Bond*; Cornell University Press: Ithaca, NY, 1906; p 255.

(33) Herzberg, G. *Molecular Spectra and Molecular Structure Volume I—Spectra of Diatomic Molecules*; Krieger Publishing Company: Malabar, Florida, 1989; Section III, p 102.

(34) James, A. M.; Kowalczyk, P.; Langlois, E.; Campbell, M. D.; Ogawa, A.; Simard, B. *J. Chem. Phys.* **1994**, *101*, 4485.

(35) Yang, D. S.; James, A. M.; Rayner, D. M.; Hackett, P. A. *J. Chem. Phys.* **1995**, *102*, 3129.

(36) Langridge-Smith, P. R. R.; Morse, M. D.; Hansen, G. P.; Smalley, R. E.; Merer, A. J. *J. Chem. Phys.* **1984**, *80*, 593.

(37) Van Zee, R. J.; Li, S.; Weltner, W. *Chem. Phys. Lett.* **1994**, *217*, 381.

(38) Moore, C. E. *Atomic Energy Levels*; Circular No. 467; Natl. Bur. Standards: Washington, DC, 1971; Vols. 1−3.

(39) Simard, B.; Presunka, P. I.; Loock, H. P.; Berces, A.; Launila, O. *J. Chem. Phys.* **1997**, *107* (2), 307.

JP809089Y